Seasonal and long-term dynamics of the upper ocean carbon cycle at Station ALOHA near Hawaii

Charles D. Keeling
Scripps Institution of Oceanography, University of California, San Diego, La Jolla, California, USA

Holger Brix
Institute of Geophysics and Planetary Physics, University of California, Los Angeles, California, USA

Nicolas Gruber
Institute of Geophysics and Planetary Physics and Department of Atmospheric and Oceanic Sciences, University of California, Los Angeles, California, USA

Received 23 January 2004; revised 27 May 2004; accepted 2 July 2004; published 15 October 2004.

[1] Long-term trends and average seasonal variability in the upper ocean carbon cycle are investigated at Station ALOHA, the site of the U.S. JGOFS Hawaii Ocean Time series program (HOT), on the basis of a 14-year time series (1988–2002) of dissolved inorganic carbon (DIC), alkalinity, and $^{13}C/^{12}C$ ratio of DIC data. Salinity-normalized DIC (sDIC) and computed oceanic pCO_2 show distinct upward trends of 1.2 ± 0.1 μmol kg^{-1} yr^{-1} and 2.5 ± 0.1 μatm yr^{-1}, respectively, while the $^{13}C/^{12}C$ isotopic ratio of DIC (expressed as $\delta^{13}C^{oc}$) decreases at a mean rate of -0.027 ± 0.001‰ yr^{-1}. More than half of the rates of change in sDIC and oceanic pCO_2, and most of the change in $^{13}C/^{12}C$, are attributed to the uptake of isotopically light anthropogenic CO_2 from the atmosphere. The residual trends appear to be caused mainly by a regional change in the net freshwater budget, perhaps associated with a regime change of the North Pacific climate system near 1997. Computed oceanic pCO_2 is below atmospheric pCO_2 for nearly the entire year, leading to an annual mean surface ocean pCO_2 undersaturation of about 18 μatm, and to an annual uptake of CO_2 from the atmosphere, which we compute to be 1.0 ± 0.1 mol m^{-2} yr^{-1}. We estimate that about 30% of this flux relates to the uptake of anthropogenic CO_2, and the remainder to biologically mediated export of organic carbon. Using a modified version of the diagnostic model of *Gruber et al.* [1998], constrained by $\delta^{13}C^{oc}$, we infer net community production of organic carbon (NCP) to be the dominant process generating the observed seasonal variability in sDIC. The annual integral of NCP, 2.3 ± 0.8 mol m^{-2} yr^{-1}, is comparable to previous estimates of biological production in the subtropical North Pacific. Annually integrated fluxes of air-sea gas exchange and NCP at Station ALOHA are each about two thirds of those computed for the upper ocean near Bermuda using similar methods of estimation [*Gruber et al.*, 1998, 2002]. However, the seasonal amplitudes of sDIC and $\delta^{13}C^{oc}$ near Hawaii are only half as large as near Bermuda, because air-sea gas exchange and NCP tend to oppose each other near Hawaii, but reinforce each other near Bermuda. *INDEX TERMS:* 4215 Oceanography: General: Climate and interannual variability (3309); 4805 Oceanography: Biological and Chemical: Biogeochemical cycles (1615); 4806 Oceanography: Biological and Chemical: Carbon cycling; 4870 Oceanography: Biological and Chemical: Stable isotopes; *KEYWORDS:* long-term trends, North Pacific, seasonal carbon cycle

Citation: Keeling, C. D., H. Brix, and N. Gruber (2004), Seasonal and long-term dynamics of the upper ocean carbon cycle at Station ALOHA near Hawaii, *Global Biogeochem. Cycles*, *18*, GB4006, doi:10.1029/2004GB002227.

1. Introduction

[2] The role of the world oceans in the global carbon cycle, and particularly their role as a sink for anthropogenic CO_2, has been the subject of continuing research over the last 50 years, but reliable methods to measure inorganic carbon in the ocean have become broadly available only in the last 2 decades [*Sabine et al.*, 1997; *Wallace*, 2001]. Also, most of what has been learned about the large-scale distribution of carbon in the oceans stems from one-time snapshots, usually interpreted as reflecting the long-term

0886-6236/04/2004GB002227

"climatological mean state" of the system [*Wallace*, 2001]. The awareness is growing, however, that these snapshots might provide a biased representation of this mean state, as the oceanic carbon cycle displays substantial interannual to decadal variability both in near-surface waters [e.g., *Feely et al.*, 1999; *Gruber et al.*, 2002; *Takahashi et al.*, 2003; *Dore et al.*, 2003] as well as at depth [e.g., *Bates et al.*, 2002]. Although these variations confound the identification of the long-term mean state, and the anthropogenic perturbation of the oceanic carbon cycle, they permit us to investigate the sensitivity of the marine carbon cycle to changes in external forcing, and perhaps will reveal to us how the oceanic carbon cycle might respond to future climate change [*Heimann*, 1995].

[3] Long-term time series observations at fixed sites are critical for documenting these variations and identifying the processes underlying them. However, due to the large efforts necessary to establish and maintain such time series, few records of oceanic carbon variability are yet available. Of note are two continuing efforts established in 1988 as part of the U.S. Joint Ocean Global Flux Studies (JGOFS) program [*Lomas et al.*, 2002]: the Bermuda Atlantic Time series (BATS) [*Michaels and Knap*, 1996] and the Hawaii Ocean Time series (HOT) program [*Karl and Lukas*, 1996]. Both time series sites are located within subtropical gyres, members of an oceanic regime covering about 40% of the Earth's surface. Together they constitute the world's largest distinct oceanic ecosystem. The North Pacific Subtropical Gyre (NPSG) is the more extensive of these gyres, with a surface area of approximately 2×10^7 km^2. Atmospheric CO_2 inversion studies [*Gurney et al.*, 2002] and basin-wide measurements of the partial pressure of CO_2 (pCO_2) near the sea surface [*Takahashi et al.*, 2002] have suggested that the NPSG is a substantial sink for atmospheric CO_2, but the magnitude of this sink and its underlying mechanisms are not well known [*Winn et al.*, 1994]. Moreover, *Dore et al.* [2003] have documented recently that its magnitude may have decreased over the last decade, possibly due to a reduction in rainfall that caused a change in the surface ocean freshwater budget. There is also evidence that biological production in the NPSG has recently undergone a shift from nitrogen to phosphorus limitation [*Karl*, 1999; *Karl et al.*, 2001], but the implications of these findings on the upper ocean carbon cycle are unclear.

[4] We address these implications by investigating the upper oceanic carbon cycle near Hawaii and its controlling processes on timescales from seasonal to decadal on the basis of a newly reported 14-year inorganic carbon data set from Station ALOHA, the site of the HOT program. This time series is based on water samples taken from the oceanic mixed layer between 1988 and 2002 and analyzed in the shore laboratory of the Carbon Dioxide Research Group (CDRG) at the Scripps Institution of Oceanography. This data set encompasses measurements of DIC, titration alkalinity (Alk), and the $^{13}C/^{12}C$ ratio of DIC. The latter is expressed by the reduced ratio

$$\delta^{13}C = \frac{^{13}C/^{12}C}{^{13}C/^{12}C|_{std}} - 1, \quad (1)$$

where $^{13}C/^{12}C\,|_{std}$ denotes the $^{13}C/^{12}C$ ratio of the Pee Dee belemnite standard [*Craig*, 1957; *Mook and Grootes*, 1973]. We will refer to the $^{13}C/^{12}C$ ratio of DIC as $\delta^{13}C^{oc}$ to distinguish it from the $^{13}C/^{12}C$ ratio of atmospheric CO_2, $\delta^{13}C^{atm}$.

[5] In this paper, we focus on the mean seasonal cycle and on the approximately decadal long-term trend. Shorter-term interannual variability is discussed in a companion paper by *Brix et al.* [2004]. Both papers significantly extend the data and discussion from the initial study by *Keeling* [1993], who reported results from our measurement program from 1988 to 1991. In order better to understand the mechanisms that generate seasonal variability, we employ a slightly revised version of the diagnostic box model of *Gruber et al.* [1998], which permits us to deduce quantitatively how biological processes, air-sea gas exchange, lateral transport, entrainment, and vertical diffusion influence the oceanic carbon cycle in the mixed layer.

[6] First, in section 2, we review current knowledge of the carbon cycle in the subtropical North Pacific Ocean and identify key questions to be addressed. Section 3 then describes our data sets obtained at Station ALOHA. Thereafter, we investigate long-term trends, in section 4, and seasonal variations in section 5. Implications of these results are discussed in section 6, with a focus on biological production, air-sea gas exchange, and relative importance of lateral versus vertical transport. Finally, in section 7, we compare our findings with previous results from the North Atlantic subtropical gyre, and put our results into the broader context of the global oceanic carbon cycle.

2. Carbon Cycling in the North Pacific Subtropical Gyre

[7] Station ALOHA is located at 22°45′N, 158°00′W, within the southern limb of the anti-cyclonic North Pacific subtropical gyre (NPSG), with the large-scale geostrophic flow coming predominantly from northeasterly directions [*Tomczak and Godfrey*, 2003]. Ekman drift, induced by the northeasterly trade winds, causes a surface intensified flow in northwesterly direction, superimposing on this geostrophic flow. The expected total surface flow is therefore easterly with either a weak northward or southward component. Surface drifter observations north of the Hawaiian island chain show easterly flow, with a small and variable northward component [*Johnson*, 2001]. Station ALOHA lies approximately 100 km north of the island of Oahu, about twice a Rossby radius from the steep topography associated with the Hawaiian ridge [*Karl and Lukas*, 1996]. The station is characterized year-round by a relatively shallow mixed layer (20–120 m) [*Karl and Lukas*, 1996] and a deep nutricline, leading to nearly permanently low concentrations of inorganic nutrients in the upper mixed layer [*Karl and Lukas*, 1996]. The cycling of inorganic carbon there has been reported by *Keeling* [1993], *Winn et al.* [1994], *Sabine et al.* [1995], *Winn et al.* [1998], *Dore et al.* [2003], and *Quay and Stutsman* [2003]. We summarize their results here, highlighting still unresolved questions.

[8] Despite relatively small seasonality in meteorological forcing, the near-surface oceanic carbon cycle at Station

ALOHA shows distinct seasonal variations [*Keeling*, 1993; *Winn et al.*, 1994, 1998; *Quay and Stutsman*, 2003]. Between late winter and late summer, dissolved inorganic carbon (DIC) decreases by 15 to 20 μmol kg^{-1} while $\delta^{13}C^{oc}$ increases by about 0.1‰. *Winn et al.* [1994], analyzing oceanic carbon data for the first 4 years of the Station ALOHA time series data set, suggested that this drawdown is caused by the advection of relatively warm water, low in DIC, from the eastern and tropical Pacific Ocean during the summer.

[9] In contrast, *Quay and Stutsman* [2003] pointed out that the nearly simultaneous increase of $\delta^{13}C^{oc}$ indicates that NCP (net community production, defined as net autotrophic production minus community respiration [*Williams*, 1993]) must contribute substantially to the winter to summer decrease in DIC, as no other process can cause a drawdown of DIC while increasing $\delta^{13}C^{oc}$. They demonstrated this using a diagnostic box modeling approach similar to that which we employ in our study here. They also showed that lateral transport contributes to this drawdown as well, whereas air-sea gas exchange, vertical transport, and mixing oppose it. Over the annual cycle, they found that NCP removes 2.5 ± 1.2 mol m^{-2} yr^{-1} from the mixed layer and that this loss is nearly balanced by an upward DIC transport of 2.4 ± 1.8 mol m^{-2} yr^{-1}.

[10] While their estimate of NCP is within the range of previously published estimates, they needed to invoke a large vertical flux of DIC into the surface mixed layer in order to balance loss stemming from NCP. They argued that this transport occurs by diffusion, and that the effective vertical diffusivity at the base of the mixed layer is about a factor of 10 larger than estimated on the basis of the vertical stability of the water column, possibly in response to episodic events such as eddies and storms. However, it is conceivable that *Quay and Stutsman* [2003], by associating horizontal transport of DIC solely to climatological mean geostrophic and Ekman mass transport, may have underestimated episodic lateral inputs of DIC and consequently overestimated the effects of vertical diffusion on DIC. For example, eddies, storms, and other episodic events may contribute not only to increased vertical diffusivities, but to elevated horizontal transport of inorganic carbon as well.

[11] Several authors have pointed out that the ocean near Hawaii acts as a sink for atmospheric CO_2 [*Keeling*, 1993; *Winn et al.*, 1998; *Dore et al.*, 2003; *Quay and Stutsman*, 2003]. *Winn et al.* [1994] proposed that this sink is caused primarily by the northward advection of waters from the equator that take up CO_2 from the atmosphere as these waters are deficient in DIC as a result of strong outgassing near the equator. We will propose here an alternative explanation that suggests that most of the uptake of atmospheric CO_2 is likely to be owing to the export of organic matter. Part of this sink must be owing to the uptake of anthropogenic CO_2 as well, but its magnitude relative to natural causes of air-sea exchange remains uncertain.

[12] The upper ocean carbon cycle at Station ALOHA exhibits distinct long-term trends. *Winn et al.* [1998] reported that DIC increased there at a rate of about 1 μmol kg^{-1} per year from 1988 to 1995 and argued that nearly all of the uptake was of anthropogenic CO_2 from the atmosphere. *Dore et al.* [2003] have pointed out recently that surface oceanic pCO_2 increased at a rate of 2.5 ± 0.3 μatm yr^{-1} between 1988 and 2001, exceeding the rate of rise of atmospheric CO_2 of about 1.5 μatm yr^{-1}. *Dore et al.* [2003] suggested that this higher rate of increase in oceanic pCO_2 is related to an increase in surface salinity, possibly caused by a reduction in rainfall. However, this explanation does not fully account for how a change in the surface freshwater budget could cause this unexpected rise in surface ocean pCO_2. *Dore et al.* [2003] also did not investigate how this salinity change might be connected to larger-scale climate patterns.

[13] Several questions remain about the seasonal and long-term behavior of the near-surface ocean carbon cycle near Hawaii. What are the relative roles of biology and physical processes in generating the seasonal drawdown from spring to summer? Which identified mechanisms are mainly responsible for supplying the carbon that is exported from the mixed layer? Also, how large is the uptake of CO_2 from the atmosphere, and what process maintains this sink? Why have DIC and pCO_2 near Hawaii risen more rapidly than expected from uptake of anthropogenic CO_2, and to what degree are these trends local or related to large-scale climate modes? We will address these questions with an inorganic carbon data set spanning 14 years, a time series surpassed in length only by the now nearly 20-year record for waters near Bermuda [*Gruber et al.*, 2002].

3. Data

[14] Samples were taken at Station ALOHA from depths of approximately 5 m and 25 m in duplicate during most HOT cruises from their beginning in 1988 until present. These samples were shipped to La Jolla and analyzed in the laboratories of the Carbon Dioxide Research Group (CDRG) at the Scripps Institution of Oceanography. Uniform measurement procedures for DIC, Alk, and the $^{13}C/^{12}C$ ratio of DIC were used, as explained in Appendix A. To remove the effects of fresh water fluxes, DIC and Alk are normalized to a constant salinity of 35, approximately the long-term mean of sea surface salinity at Station ALOHA (salinity is expressed on the practical salinity scale without units [*U.N. Educational, Scientific, and Cultural Organization*, 1981]). These quantities will be denoted as sDIC and sAlk, respectively. Up to 1999, samples were analyzed at both depths, and subsequently only at 5 m.

[15] Time series are plotted in Figures 1a–1d. The data agree well with corresponding measurements made as part of the JGOFS HOT program by *Dore et al.* [2001], who analyzed a subset of the CDRG samples (for 1988 to 1999) and found a mean difference of −0.01 ± 2.98 μmol kg^{-1} for DIC and 0.36 ± 5.73 μmol kg^{-1} for Alk (±1 standard deviation). Figure 1d depicts the partial pressure of surface ocean CO_2 (pCO_2^{oc}), calculated from DIC and Alk and from temperature, salinity (plotted in Figure 2), and nutrients as described by *U.S. Department of Energy* (*DOE*) [1994]. The calculations employ a thermodynamic model of the carbonate system and use the dissociation constants of *Mehrbach et al.* [1973] as reformulated on the total hydrogen scale by *Lueker et al.* [2000]. This choice of dissociation constants is

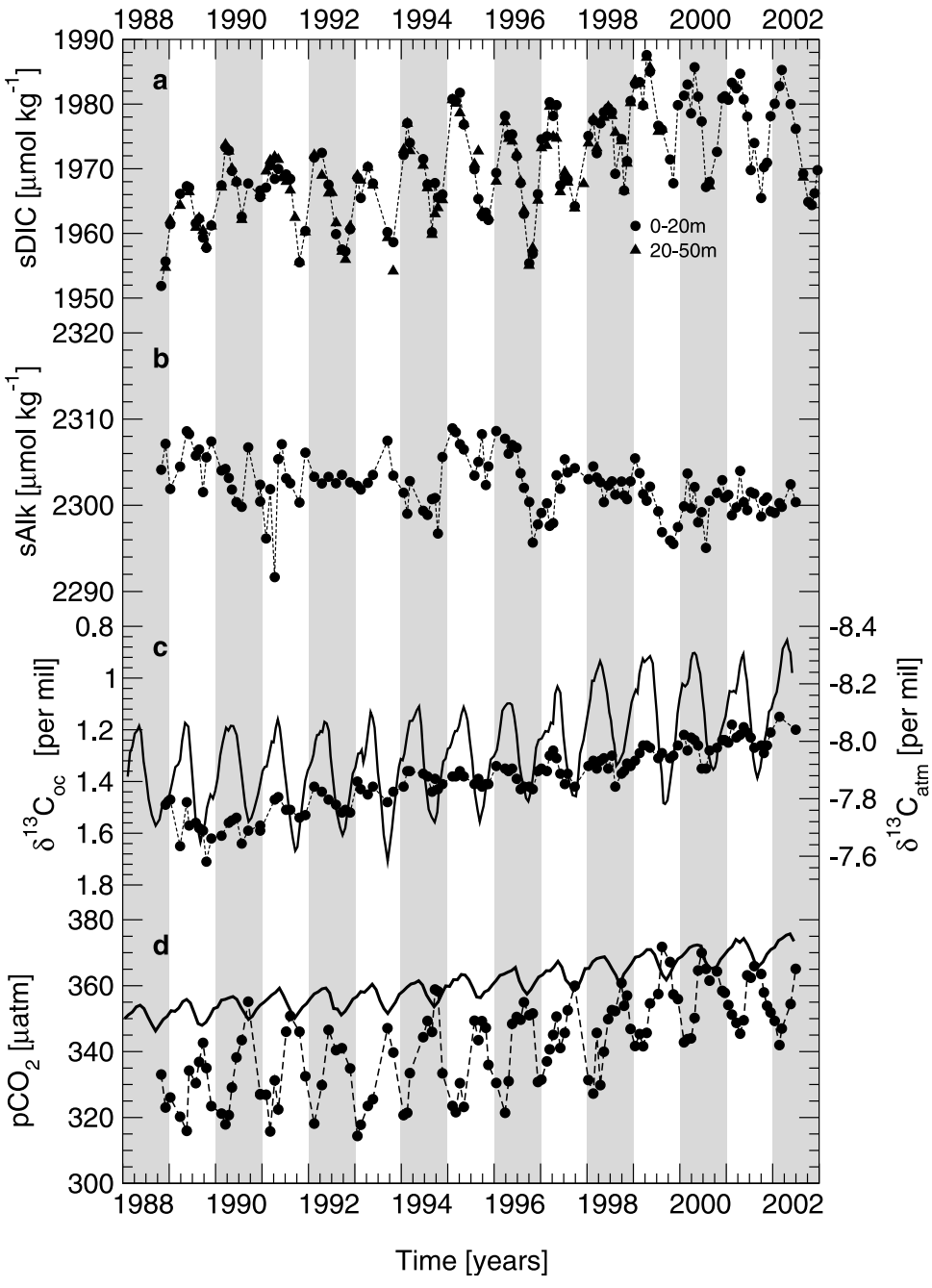

Figure 1. Time series of inorganic carbon parameters at Station ALOHA from 1988 to 2002. (a) Dissolved inorganic carbon (sDIC) normalized to a salinity of 35.0. (b) Similarly normalized total alkalinity (sAlk). (c) $\delta^{13}C$ of surface ocean DIC (circles) and of atmospheric CO_2 (solid line) at Cape Kumukahi, Hawaii (*Keeling et al.* [1989] and updates) (scales are inverted). (d) Calculated pCO_2 using dissociation constants after *Mehrbach et al.* [1973]. The thick line depicts atmospheric pCO_2 computed from monthly mean xCO_2 data (measured at Cape Kumukahi (*Keeling et al.* [1989] and updates)) using monthly mean surface air temperatures and a long-term mean value for atmospheric pressure at Station ALOHA.

consistent with results of *Lee et al.* [2000a], but is only loosely supported by a comparison of our computed pCO_2 with underway pCO_2 measurements collected during HOT cruises from September 1996 until May 1998 (John Dore, personal communication, 2003), which show a mean difference of 3.6 ± 5.7 µatm (pCO_2 computed by CDRG higher than those measured underway). Atmospheric pCO_2 (thick line in Figure 1d) was computed from the measured dry air mixing ratios at Cape Kumukahi (see *Keeling et al.* [1989] and updates) using the mean atmospheric pressure

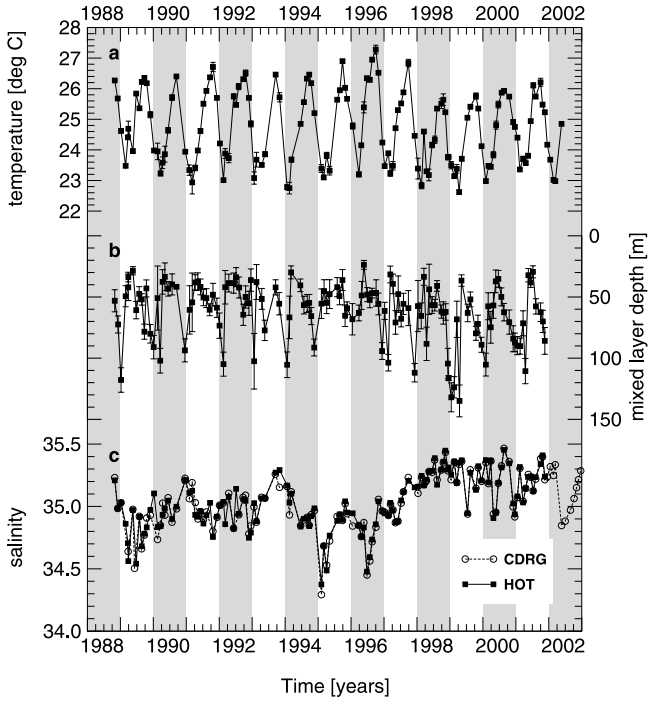

Figure 2. Time series of physical parameters at station ALOHA site from 1988 to 2002. (a) Temperature, (b) estimated mixed layer depth (see text), and (c) salinity. Open circles in Figure 2c denote measurements done by the Oceanographic Data Facility of the Scripps Institution of Oceanography on the samples returned from Station ALOHA. All other data are from the HOT program [*Lukas and Karl*, 1999]. Temperature and salinity are averages of the upper 20 m. Error bars denote the 1-σ standard deviation of the mean values during a particular station occupation.

(1018 hPa) observed at Station ALOHA. The calculation of both atmospheric and oceanic pCO_2 takes into consideration the pressure contribution from water vapor, assumed in both phases to be at 100% saturation with the surface ocean temperature and salinity [*DOE*, 1994]. As noted above, oceanic pCO_2 lies almost always below atmospheric pCO_2.

[16] Surface mixed layer temperature (T) and salinity (S) were determined by calculating the averages of all conductivity, temperature, and depth (CTD) observations in the upper 20 m (Figures 2a and 2c) from the HOT program [*Lukas and Karl*, 1999]. The depth of the mixed layer, h, was estimated from CTD data applying a variable potential density criterion proposed by *Sprintall and Tomczak* [1992], which assumes a temperature difference between the surface and the base of the mixed layer of 0.5°C. All casts for a particular station occupation were then averaged (Figure 2b).

4. Long-Term Trends

[17] Salinity-normalized concentration of DIC (sDIC), $\delta^{13}C^{oc}$, and pCO_2^{oc} in the CDRG data for near-surface water all show distinct long-term linear trends. From October 1988 to June 2002, sDIC increased on average by 1.22 ± 0.08 μmol kg^{-1} yr^{-1}, and oceanic pCO_2 by 2.5 ± 0.1 μatm yr^{-1}, while $\delta^{13}C^{oc}$ decreased by −0.027 ± 0.001‰ yr^{-1} (see Figure 1 and Table 1). The trend in salinity-normalized alkalinity (sAlk) was small (−0.32 ± 0.06 μmol kg^{-1} yr^{-1}), contrasting with an upward trend for Alk of 1.30 ± 0.23 μmol kg^{-1} yr^{-1}. This difference is driven by a strong increase in salinity, which exhibits a long-term mean trend of 0.026 ± 0.004, which also explains the higher trend in DIC (2.64 ± 0.25 μmol kg^{-1} yr^{-1}) relative to sDIC. We first discuss the trends for sDIC, DIC, and pCO_2.

4.1. Trends in Inorganic Carbon

[18] The linear upward trends for sDIC and pCO_2 in the CDRG data are statistically indistinguishable from those obtained independently by *Dore et al.* [2003] for the period from October 1988 through December 2001 (1.19 ± 0.14 μmol kg^{-1} yr^{-1} and 2.5 ± 0.3 μatm yr^{-1}, respectively). An upward trend for pCO_2 for near-surface waters in the subtropical gyres is expected, as these waters tend to equilibrate with the anthropogenic perturbation of rising atmospheric CO_2. However, at Station ALOHA the upward oceanic pCO_2 trend substantially exceeds that of atmospheric pCO_2 as observed near sea level on the coast of Hawaii (1.5 ± 0.0 μatm yr^{-1}), with the air-sea difference,

Table 1. Long-Term Data Trends for Station ALOHA and Station "S"/BATS[a]

Parameter	Unit	Mean ALOHA	Trend/Year 1988–1996 ALOHA[b]	Trend/Year 1997–2002 ALOHA[b]	Trend/Year 1988–2002 ALOHA[b]	Trend/Year 1983–2001 Station "S"/BATS[c]
sDIC	μmol kg^{-1}	1971.05	0.90 ± 0.15	1.16 ± 0.29	1.22 ± 0.08	0.64 ± 0.05
DIC	μmol kg^{-1}	1973.58	−0.24 ± 0.46	2.17 ± 0.77	2.64 ± 0.25	
sAlk	μmol kg^{-1}	2302.30	−0.04 ± 0.14	−0.32 ± 0.18	−0.32 ± 0.06	−0.02 ± 0.01
Alk	μmol kg^{-1}	2306.23	−0.64 ± 0.47	0.85 ± 0.78	1.30 ± 0.23	
$\delta^{13}C^{oc}$	‰	1.389	−0.030 ± 0.002	−0.031 ± 0.002	−0.027 ± 0.001	−0.024 ± 0.001
$\delta^{13}C^{atm}$	‰	−7.983‰	−0.015 ± 0.000	−0.020 ± 0.000	−0.023 ± 0.000	
pCO_2^{oc}	μatm	341.8	1.4 ± 0.2	3.2 ± 0.4	2.5 ± 0.1	1.5 ± 0.1
$pCO_2^{atm\ d}$	μatm	360.5	1.3 ± 0.0	1.8 ± 0.0	1.5 ± 0.0	
T	°C	24.74	0.02 ± 0.02	0.05 ± 0.04	−0.02 ± 0.01	0.03 ± 0.01
S	pract. scale	35.038	−0.017 ± 0.008	0.018 ± 0.012	0.026 ± 0.004	0.008 ± 0.005
h	m	61.50	0.30 ± 0.58	0.45 ± 1.89	1.31 ± 0.35	

[a]Uncertainties (±) represent 1 standard deviation. Values are from October 1988 until June 2002 unless otherwise stated. The trends were calculated from deseasonalized data (obtained by subtracting harmonic fits).
[b]Data for mixed layer depth, h, do not include 2002.
[c]From *Gruber et al.* [2002].
[d]Atmospheric data from Cape Kumukahi range from January 1988 until June 2002.

Table 2. Contribution of Different Variables to the Observed Long-Term Trend of DIC at Station ALOHA[a]

Term[b]	Period 1988–1996	1997–2002	1988–2002
Individual Terms			
ΔT	−0.14 ± 0.40	−0.39 ± 0.66	+0.17 ± 0.19
ΔS	+0.10 ± 0.09	−0.11 ± 0.14	−0.15 ± 0.05
ΔS (dilution)	−0.79 ± 0.75	+0.84 ± 1.12	+1.21 ± 0.37
Δ sAlk	−0.03 ± 0.20	−0.23 ± 0.25	−0.23 ± 0.08
ΔpCO_2^{atm}	+0.80 ± 0.03	+1.05 ± 0.06	+0.93 ± 0.02
$-\Delta\Delta pCO_2$[c]	+0.05 ± 0.29	+0.86 ± 0.53	+0.56 ± 0.15
Sum of Terms Versus Observed			
Σ[d]	−0.02 ± 0.92	+2.03 ± 1.43	+2.49 ± 0.46
ΔDIC_{obs}[e]	−0.24 ± 0.46	+2.17 ± 0.77	+2.64 ± 0.25

[a]Values are in μmol kg^{-1} yr^{-1}. Uncertainties have been calculated using 2σ errors from Table 1, applying a quadratic error propagation.

[b]Symbols represent the entire term, including the partial derivatives (see equation (2)).

[c]The $\Delta\Delta pCO_2 = \Delta(pCO_2^{atm} - pCO_2^{oc})$ term is multiplied with −1 to reflect its contribution to the DIC budget correctly.

[d]Σ is the sum of all five terms, ΔDIC_{obs} is the observed trend in DIC.

[e]Partial derivatives were computed around the long-term mean values of the different parameters, while keeping all other parameters constant. The following values were obtained: $\partial DIC/\partial T$ = −8.7 μmol kg^{-1} (°C)$^{-1}$; $\partial DIC/\partial pCO_2^{oc}$ = 0.6 μmol kg^{-1} μatm^{-1}; $\partial DIC/\partial S$ = −5.9 μmol kg^{-1}; $(sAlk/S_0)(\partial DIC/\partial Alk)$ = 46.7 μmol kg^{-1}; $\partial DIC/\partial Alk$ = 0.71 μmol kg^{-1} (μmol kg^{-1})$^{-1}$.

which averages about 18 μatm, decreasing from about 20 μatm in 1989 to 14 μatm in 2002. A remarkably low mean air-sea pCO_2 difference in 1999 coincides with a marked increase in salinity that began in 1997 (see Figure 1).

[19] This elevated trend in oceanic pCO_2 is a result of the observed trends in DIC, Alk, and/or salinity, because the temperature trend is small (Table 1). Given the observation that oceanic pCO_2 changes about 9 μatm per 1 unit salinity change given constant DIC and Alk [*Sarmiento and Gruber*, 2004], the direct impact of the observed salinity increase on pCO_2 can only explain part of the trend (about 0.2 μatm yr^{-1}). The observed strong increases in DIC and Alk (Table 1) have opposite effects on oceanic pCO_2. While an increase in DIC increases oceanic pCO_2, an increase in Alk decreases it. Thus the observed increase in pCO_2 beyond that expected from the uptake of anthropogenic CO_2 must be primarily driven by the trend in DIC overwhelming the negative oceanic pCO_2 trend induced by the increase in Alk. Comparing the trends of Alk with sAlk and that of DIC with sDIC reveals that almost the entire trend in Alk and more than half of the trend in DIC are a consequence of a change in the upper ocean freshwater balance as reflected in the salinity increase. As the net effect of the removal of freshwater leads to an increase in oceanic pCO_2 [*Sarmiento and Gruber*, 2004], this mechanism represents a significant contribution to the increase in oceanic pCO_2, as noted by *Dore et al.* [2003]. The remaining trend in oceanic pCO_2 comes from the trend in sDIC, part of which is associated with the uptake of anthropogenic CO_2 from the atmosphere. It turns out, however, that the observed rate of increase of sDIC (1.22 ± 0.08 μmol kg^{-1} yr^{-1}) is larger than that expected from this uptake (about 0.93 ± 0.02 μmol kg^{-1} yr^{-1}; see Table 2). Therefore, in order to understand the strong upward trend in oceanic pCO_2, we not only need to explain the causes for the changes in the freshwater balance affecting DIC and Alk, but also the cause of the upward trend in sDIC that is not associated with anthropogenic CO_2. Rather than focusing just on sDIC, we investigate the trend in DIC, permitting us to discuss all factors simultaneously.

[20] Possible external causes for changing DIC beyond that expected from anthropogenic CO_2 are changes in temperature, salinity, and Alk. Variations in salinity affect DIC in two ways. Directly, along with temperature and Alk, salinity influences ionic dissociation constants, changing the equilibrium concentration of DIC for given magnitudes of pCO_2, Alk, and salinity. Also, indirectly, it reflects the addition or removal of freshwater, altering the concentration of DIC and Alk. As seen above, the trend for sAlk is small, and that for temperature is negligible. Thus changes in the freshwater budget are likely to be the primary external cause, besides anthropogenic CO_2, to have contributed to changes in DIC, as proposed by *Dore et al.* [2003]. We will also see that there appears to be a component to this increase that is driven by a water mass change.

[21] To investigate quantitatively how external factors influence the observed change in DIC, we express the total change in DIC over a given period, ΔDIC, as the sum of separate changes arising from varying sea surface temperature (ΔT), salinity (ΔS), salinity-normalized alkalinity (ΔsAlk), atmospheric pCO_2 (ΔpCO_2^{atm}), and the air-sea pCO_2 difference ($\Delta(pCO_2^{atm} - pCO_2^{oc})$). Thus

$$\Delta DIC = \frac{\partial DIC}{\partial T}\Delta T + \frac{\partial DIC}{\partial S}\Delta S + \frac{sAlk}{S_0}\frac{\partial DIC}{\partial Alk}\Delta S + \frac{S}{S_0}\frac{\partial DIC}{\partial Alk}\Delta sAlk + \frac{\partial DIC}{\partial pCO_2^{oc}}\Delta pCO_2^{atm} - \frac{\partial DIC}{\partial pCO_2^{oc}}\Delta\left(pCO_2^{atm} - pCO_2^{oc}\right). \quad (2)$$

where S_0 = 35 denotes the normalization salinity, and where we separately accounted for the change in DIC arising from salinity-induced changes in the dissociation constants (second term) and for the change induced by the freshwater effect (third right-hand term). The partial derivatives in equation (2) are computed in the approximation that they are small differences in the neighborhood of the respective long-term mean values. To determine Δ values, the trends reported in Table 1 were multiplied by the respective time periods. See Appendix B for details on the derivation.

[22] The results of this separation of ΔDIC into components (listed in Table 2) reveal that, after accounting for an increase in DIC associated with increasing atmospheric CO_2, the dominant DIC component is the dilution term. This term includes a salinity-driven increase in alkalinity, which causes a decrease in the oceanic buffer factor (∂ ln pCO_2/∂ lnDIC) [*Takahashi et al.*, 1980], and hence a transfer of CO_2 from the atmosphere to DIC in the ocean toward maintaining chemical equilibrium with the atmosphere. The next most important term driving the long-term increase in DIC is decreasing air-sea pCO_2 difference (last term in equation (2)). This term takes into account that DIC

at Station ALOHA has increased at a rate faster than predicted by assuming equilibrium with T, S, Alk, and atmospheric pCO_2. The only means of changing this term is to alter the mean chemical state of the upper ocean carbon cycle system, a change most likely caused by a change in the predominant water mass occupying the area around Station ALOHA.

[23] A close inspection of the time series displayed in Figures 1 and 2 reveals that a disproportionally large part of these contributions to the DIC increase occurred after 1997, evidently accompanied by substantial changes in the mean seasonal cycle of temperature, with summer maxima almost 2°C lower after 1997 (Figure 2a). Near this time, a marked increase occurred in mixed layer salinity (Figure 2c). The significantly differing trends before and after 1997 for Alk, oceanic pCO_2, and S, lead to rather differently forced changes in DIC (Table 2). From 1988 to 1996, trends forced by a freshwater flux and air-sea pCO_2 difference tend to cancel, while from 1997 to 2002, they tend to reinforce. Our finding that the changes in salinity represent the main non-anthropogenic driving force for observed increase in surface ocean DIC agrees with the results of *Dore et al.* [2003], but adds additional driving processes to their analysis of changes in pCO_2.

4.2. Local Versus Large-Scale Climate Shifts

[24] *Dore et al.* [2003] argued that the observed large change in surface salinity near 1997 was driven mainly by a local decrease in rainfall altering the freshwater balance near Station ALOHA. They cite an observed reduction in rainfall at Honolulu International Airport on the island of Oahu (about 0.3 m yr^{-1}) between the periods 1988–1996 and 1997–2001 as an adequate basis to explain the salinity increase. However, for an average mixed layer depth of 60 m, as observed at Station ALOHA, this 0.3 m yr^{-1} reduction in rainfall could generate a salinity increase of only about 0.2, considerably less than the observed increase of about 0.5. We therefore suggest that changes in water masses near Station ALOHA, not necessarily related to Honolulu rainfall, contributed significantly to the salinity increase as well. This near-surface water mass change hypothesis is corroborated by the observation that the properties of waters between 100 and 200 m have undergone substantial changes as well. These waters represent Eastern North Pacific Central Water (ENPCW), whose properties are largely formed to the northwest of Hawaii [*Tomczak and Godfrey*, 2003].

[25] These changes at depth, and the persistence of the surface ocean changes after 1997, suggest that the salinity changes observed near Hawaii were owing to both a local alteration of the freshwater balance and a water mass change that took place over a wide area of the North Pacific Ocean, the latter perhaps connected to the Pacific Decadal Oscillation (PDO), which represents the most prominent mode of climate variability in the North Pacific [*Mantua et al.*, 1997]. There is indeed evidence that this climate mode underwent a "regime shift" in the late 1990s [*Mantua and Hare*, 2002; *Chavez et al.*, 2003], although the exact nature of this shift and its association with the PDO is an issue of debate currently [*Bond et al.*, 2003].

[26] To test the hypothesis that the changes observed near Hawaii around 1997 are associated with Pacific-wide changes, we calculated differences in 5-year means for 1992–1996 and 1997–2001, for sea level pressure, wind stress (National Center for Environmental Prediction (NCEP) Reanalysis data), and SST (Reynolds optimally interpolated (OI) SST data) for the Pacific Ocean north of 35°S. All data sets were provided by the NOAA-CIRES Climate Diagnostics Center, Boulder, Colorado (http://www.cdc.noaa.gov). Our calculated pentadal differences for SST and wind stress, shown in Figure 3a, reveal a systematic large-scale shift of the state of the North Pacific climate system that is consistent with our hypothesis of non-local changes. The pentadal difference pattern resembles the canonical PDO pattern (Figure 3b) [*Mantua et al.*, 1997; *Mantua and Hare*, 2002]). Both the PDO during its negative phase and the changes from 1992–1996 to 1997–2001 show a dipole structure with negative SST anomalies prevailing in the Gulf of Alaska and the eastern subtropical North Pacific, while positive SST anomalies characterize the western subtropical and temperate North Pacific. The Hawaiian islands, though not situated close to the center of action of these two patterns, are close to a region of strongly reduced SST after 1997. They are also within a region of increased northerly to northeasterly winds, extending westward from North America, to about the 180° meridian, accompanied by colder summer temperatures observed at Station ALOHA after 1997.

[27] The changes observed at Station ALOHA around 1997 appear therefore to have been a result, in part, of a large-scale shift in the climate of the North Pacific. Given the resemblance of the pentadal differences and canonical PDO patterns, this change could be related to a change in the PDO from its positive to its negative phase [*Mantua et al.*, 1997]. Support for this hypothesis comes from the observation that the changes occurred about 20 years after what appears to have been a previous PDO regime shift in 1976–1977 [*Trenberth*, 1990; *Mantua et al.*, 1997], thus consistent with the typical recurrence time of shifts in the PDO during the twentieth century as identified by *Chao et al.* [2000]. However, *Bond et al.* [2003] recently suggested that the North Pacific climate change in the late 1990s was not associated with the canonical PDO, but rather with a secondary mode of North Pacific climate variability, whose spatial pattern is slightly different than that of the PDO. The exact association of the pentadal differences shown in Figure 3a with a particular mode of North Pacific climate variability is secondary for our argument here, since the climatic forcing that possibly led to the changes near Hawaii is independent of this classification.

[28] Our analysis shows that the changes around 1996/1997 were associated with a deepening of the Aleutian low and an intensification of the high-pressure system over the subtropics. This led to a stronger wind stress over the northern North Pacific, which caused the NPSG (see arrows in Figure 3a) and the subduction region for ENPCW to shift eastward. We suspect that this eastward displacement of the NPSG in turn caused a change in water mass structure near Hawaii, in which the typically dominant temperature-salinity characteristics of the surface waters are replaced

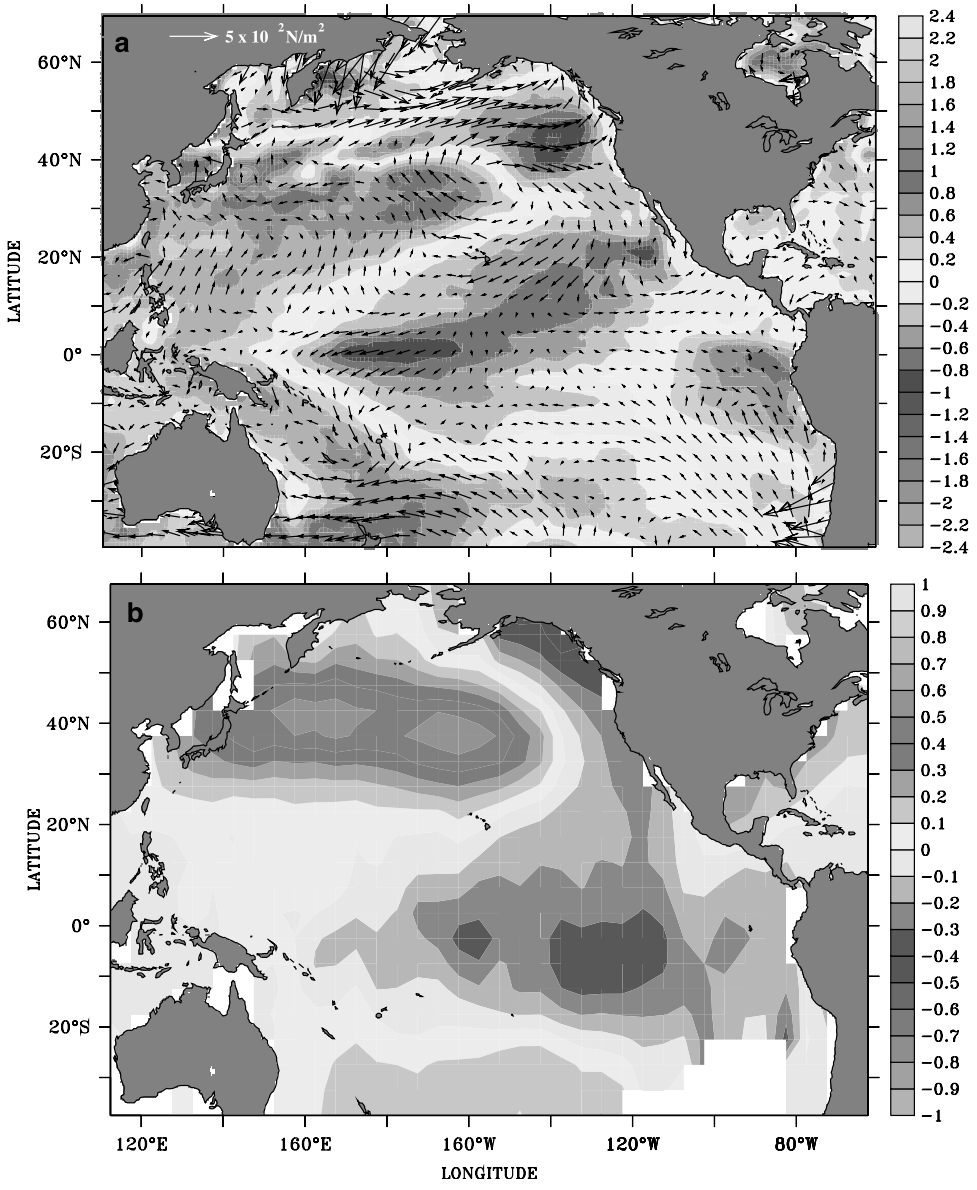

Figure 3. Pattern of climate change in the North Pacific. (a) Difference between 5-year mean SST (monthly mean Reynolds OI data in °C, shaded) and wind stress anomalies (monthly mean NCEP Reanalysis data in N/m^2, arrows) for 1997–2001 minus 1992–1996. (b) Map of the regression coefficient of SST anomalies versus a dimensionless PDO index [*Mantua et al.*, 1997]. The regression coefficient has been inverted in order to emphasize the similarity to Figure 3a. Units are °C per unit standard deviation. See text for data sources. See color version of this figure at back of this issue.

with water masses of more westerly origin, saltier and more alkaline. We therefore propose that such a water mass change near 1997 was the dominant factor causing the observed long-term change in salinity at Station ALOHA, rather than changes in the local water balance.

4.3. Oceanic ^{13}C Suess Effect

[29] Also important to our analyses of HOT data is the near-surface ocean trend in $\delta^{13}C^{oc}$, which we will refer to as the oceanic ^{13}C Suess effect [*Keeling*, 1979]. Given the irregular changes in sDIC, and pCO_2 observed over the 14-year period of our time series, it is surprising that $\delta^{13}C$ shows a near-monotonic decrease, with a mean rate of -0.027 ± 0.001‰ yr^{-1} (see Table 1) and no marked change near 1997. This trend is statistically indistinguishable from a trend reported by *Gruber et al.* [1999] for Station ALOHA from 1988 to 1996 (-0.030 ± 0.003‰ yr^{-1}) and, with two additional measurements at nearby locations, extended back to 1982 (-0.025 ± 0.002‰ yr^{-1}). This remarkably constant trend over the last 20 years is slightly larger than the global mean ^{13}C Suess effect of about -0.015 to -0.018‰ yr^{-1} [*Gruber et al.*, 1999; *Sonnerup et al.*, 2000], but close to the

trend of -0.024 ± 0.001‰ yr^{-1} for surface waters near Bermuda [*Bacastow et al.*, 1996; *Gruber et al.*, 1999, 2002]. The trends at both these locations are close to the expected trend for subtropical surface waters caused by the uptake and storage of isotopically light anthropogenic CO_2 from the atmosphere [*Gruber et al.*, 1999; *Bacastow et al.*, 1996].

[30] Why has the ^{13}C trend in subtropical surface ocean water at these two stations remained steady and close to that expected for the accumulation of anthropogenic CO_2, while the trends for sDIC and pCO_2 are sensitive to ocean chemistry changes perhaps caused by changes in water mass? First, in sharp contrast to the influence of salinity on DIC, changes in salinity have almost no impact on $\delta^{13}C^{oc}$, neither through changes in the CO_2 dissociation constants, nor through changes in Alk. Second, given the relative uniformity of $\delta^{13}C^{oc}$ in the surface ocean [*Gruber et al.*, 1999; *Gruber and Keeling*, 2001], a horizontal change in the water masses present near Station ALOHA should lead to relatively small changes in $\delta^{13}C^{oc}$, even when DIC changes are substantial. Third, due to the 10-year timescale for equilibration of the $\delta^{13}C^{oc}$ content of a surface mixed layer with atmospheric CO_2 [*Lynch-Stieglitz et al.*, 1995; *Gruber et al.*, 1999], changes in surface chemistry and atmospheric forcing are transferred into the $\delta^{13}C^{oc}$ pool only slowly. Given this relatively small sensitivity of $\delta^{13}C^{oc}$ to non-anthropogenic chemical changes, and the large anthropogenic perturbation relative to natural variations, $\delta^{13}C^{oc}$ is a particularly sensitive tracer for tracking the uptake and storage of anthropogenic CO_2.

[31] The observed trend of near-surface ocean $\delta^{13}C^{oc}$ near Hawaii is slightly higher than the trend of $\delta^{13}C$ of atmospheric CO_2 at Cape Kumukahi over the same period, i.e., about -0.023‰ yr^{-1} (see Table 1). This is surprising, since one might assume that the ocean would lag behind the atmosphere, particularly for a tracer that has a 10-year equilibration timescale between the atmosphere and ocean. As discussed by *Gruber et al.* [1999], this finding is a result of a marked change in the atmospheric CO_2 growth rate in the early 1970s. Fossil fuel CO_2 emissions increased approximately exponentially at a rate, r, of nearly 4% per year from 1945 up to that time. Thereafter, the rate slowed to about 1.1% per year. *Bacastow and Keeling* [1979] showed that after a transient in the responses to changes in r from one steady value to another, CO_2 and $\delta^{13}C$ perturbations in a globally averaged model are predicted to increase in each reservoir at the same rate r. A reduction in r after a long time interval of constant r would cause an appreciable reduction, first in the atmospheric ^{13}C-Suess effect, and then later in the oceanic one. The high growth rate for $\delta^{13}C^{oc}$ observed near Hawaii in comparison to the atmospheric growth rate is therefore a residual signal of the high growth rates of atmospheric CO_2 before the early 1970s.

4.4. Summary

[32] We have identified significant long-term increases in near-surface ocean sDIC and pCO_2 at Station ALOHA, and a long-term decrease in $\delta^{13}C^{oc}$. Within the precision of our time series data and our understanding of oceanic processes, we estimate that about two thirds of the trends in sDIC and pCO_2, and the entire trend in $\delta^{13}C^{oc}$, can be explained by the uptake of isotopically light anthropogenic CO_2 from the atmosphere. For sDIC and pCO_2 the remaining long-term variability appears to be caused by changes in water mass structure and alterations of the freshwater budget of the surface ocean near Hawaii, both of which change surface Alk, which in turn alters surface ocean DIC.

[33] Most of the larger than expected increases in sDIC and pCO_2 for the entire 14-year record occurred after 1997. We believe that the processes driving these changes are connected to a large-scale reorganization of North Pacific climate around this time. The spatial pattern of this climate reorganization is remarkably similar to the canonical PDO pattern. We therefore tentatively postulate that the water mass and freshwater balance changes near Hawaii and their impact on surface ocean CO_2 system are caused by a recent shift in the PDO, recognizing, however, that our time series is too short to reliably assess variability on timescales associated with the dominant multidecadal periodicity of the PDO. We also recognize that the spatial similarity of the pattern is insufficient evidence for this connection, and that other modes of North Pacific climate variations could have caused this change around 1997.

5. Seasonal Cycles

[34] We turn next to a consideration of the mean seasonal cycle observed at Station ALOHA over our time series. This study is motivated by the prominence of quite regular seasonal variability in our data, as shown in Figure 1, and because longer-term variations can often be understood as modifications of the mean seasonal cycle. We will focus on the relative roles of the processes that determine the observed variability.

5.1. Observations

[35] The time series of sDIC, $\delta^{13}C^{oc}$, oceanic pCO_2, temperature, and mixed layer depth (Figures 1a, 1c, 1d, 2a, and 2b) show distinct seasonal variations, while sAlk (Figure 1b) and salinity (Figure 2c) exhibit only irregular short-term changes. To investigate the mean seasonal cycle in greater detail, we remove a linear trend from the full data set and aggregate the adjusted data into a single composite year, taking no account of interannual variations. To characterize the mean seasonal cycle, we fit to the detrended data a three-harmonic curve with periods of 12, 6, and 4 months.

[36] The average seasonal cycle of sDIC (Figure 4a), as depicted by the data points, shows a maximum near 1 April, followed by a steady drawdown to a minimum in October. This is followed by a sharp rise until January, and then a slow increase to the next maximum. The amplitude of the harmonic fit cycle is about 15 μmol kg^{-1}. Although the $\delta^{13}C^{oc}$ data exhibit more scatter relative to the seasonal cycle, they show a distinct average seasonal cycle approximately anti-phased to that of sDIC, with an amplitude of about 0.09‰ (Figure 4b). The harmonic extrema in $\delta^{13}C^{oc}$ precede by a few weeks those in sDIC. The harmonic average seasonal cycle of oceanic pCO_2 (Figure 4c) shows a maximum in September, and a more definite minimum near March with a mean amplitude of about 20 μatm.

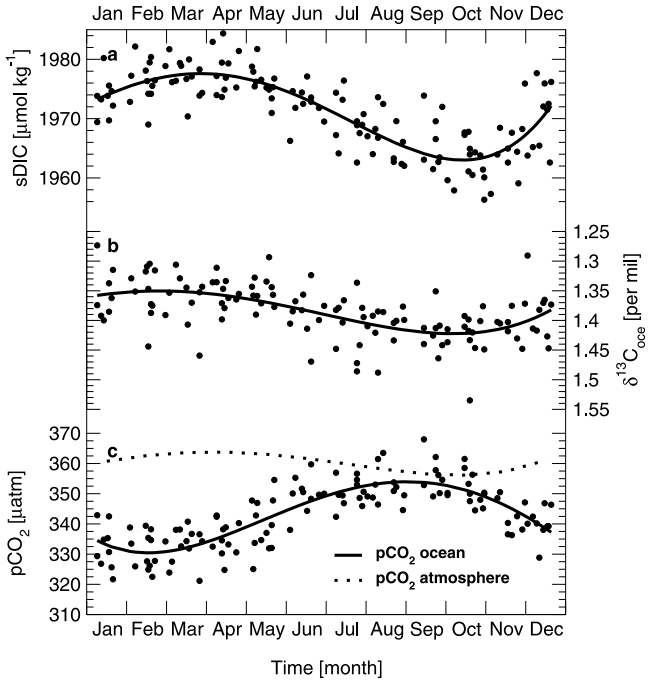

Figure 4. Linearly detrended annual composite time series of (a) sDIC, (b) $\delta^{13}C^{oc}$ (inverted scale), and (c) calculated pCO_2 at station ALOHA for the years 1988 to 2001. Symbols represent the observations described in this paper, and the solid smoothed curves depict third-order harmonic fits. Also shown in Figure 4c is a third-order harmonic fit to atmospheric CO_2 observations from Cape Kumukahi (*Keeling et al.* [1989] and updates).

Oceanic pCO_2 as depicted by the data points is undersaturated with regard to atmospheric CO_2, except in late summer and early autumn, with an annual mean undersaturation of about 18 μatm.

[37] To analyze the relative importance of the effects of temperature and DIC changes on the seasonal cycle of pCO_2, we separate the observed pCO_2 into isochemical and isothermal terms [cf. *Keeling*, 1993],

$$pCO_2^{obs}(\mathrm{DIC}, T) = \overline{(pCO_2)} + \frac{\partial pCO_2}{\partial T}\left(\overline{T} - T\right) + \frac{\partial pCO_2}{\partial \mathrm{DIC}}\left(\overline{\mathrm{DIC}} - \mathrm{DIC}\right), \quad (3)$$

where the overbars represent annual means. The second right-hand term of equation (3) describes the modulation of the mean pCO_2 due to temperature changes while keeping DIC constant (isochemical pCO_2). The third such term represents the influence of DIC changes on the seasonal cycle of pCO_2 while keeping temperature constant (isothermal pCO_2). To determine the isochemical term, we used the experimentally determined temperature sensitivity factor, $\partial \ln pCO_2/\partial T = 0.0423^{\circ}C^{-1}$ [*Takahashi et al.*, 1993]. The isothermal term was determined by difference.

[38] The isochemical pCO_2 is characterized by a maximum near October and a minimum in March, a difference of nearly 50 μatm (Figure 5). The seasonal cycle of isothermal pCO_2 has a phase approximately opposite to that of isochemical pCO_2, but an amplitude less than half of the isochemical. These results confirm the findings of *Keeling* [1993] that the seasonal cycle of pCO_2 near Station ALOHA is dominated by temperature variability, but that the pCO_2 amplitude is moderated by the spring to summer reduction of DIC.

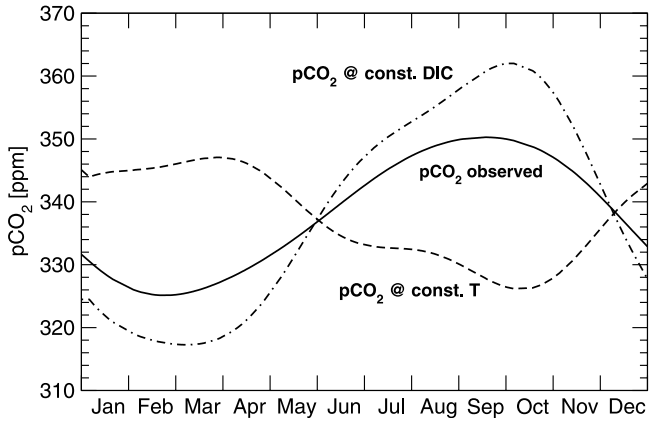

Figure 5. Contribution of temperature and DIC changes to the mean seasonal cycle of pCO_2. The dash-dotted curve represents the temperature contribution (pCO_2 at constant DIC), while the dashed curve represents the DIC contribution (pCO_2 at constant T). The solid curve is the observed mean seasonal cycle of pCO_2. For details see text.

[39] The seasonal evolution of the mixed layer depth (Figure 6b) is primarily governed by heat exchange with the atmosphere and wind stress at the ocean's surface [*Large et al.*, 1994]. Strong wind events with a large influence on the mixed layer tend to occur episodically, causing an irregular seasonal cycle (see also Figure 2b). Nevertheless, a shallow mixed layer occurs from June until October, with depths of less than 60 m during all years of

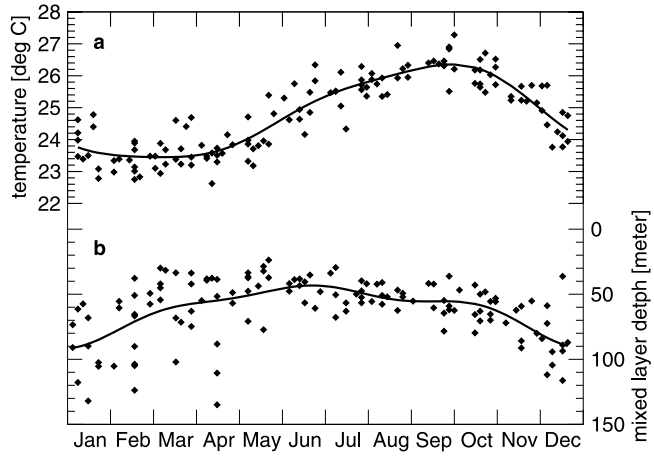

Figure 6. Detrended annual composite time series (a) of temperature and (b) of estimated mixed layer depth. Symbols represent observations from the HOT core program [*Lukas and Karl*, 1999]. The smoothed curves represent third-order harmonic fits.

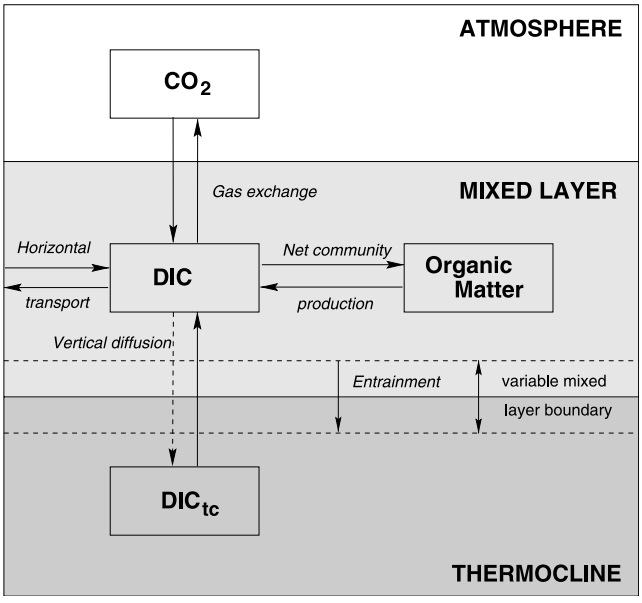

Figure 7. Schematic representation of the one-dimensional, two-box ocean model employed in the diagnostic study. Dissolved inorganic carbon is explicitly modeled only in the mixed layer. The other carbon reservoirs are only included to establish boundary conditions. The lower boundary of the mixed layer is permitted to move up and down, thereby detraining or entraining waters from the thermocline box.

our observations. In autumn, the layer gradually deepens as a result of cooling and increased wind stress. The mixed layer reaches its greatest depths during winter with a winter average of approximately 100 m and extrema of up to 140 m.

5.2. Diagnostic Model

[40] The anti-phasing of the mean seasonal cycle of sDIC and $\delta^{13}C^{oc}$, as *Quay and Stutsman* [2003] point out, suggests that net community production (NCP) plays an important role in drawing down carbon from the spring to the fall. However, the presence of a nearly continuous undersaturation clearly implies a substantial uptake of CO_2 from the atmosphere, tending to counteract this biologically induced drawdown. Also, although the seasonal cycle of DIC is strongly affected by horizontal and vertical transport and by mixing processes, their relative contributions are not readily distinguished.

[41] Separating the contributions of these various processes to the seasonal sDIC variability is difficult, as some of these processes, particularly NCP, defy simple parameterizations. We are aided, however, by the availability of simultaneous measurements of $\delta^{13}C^{oc}$ and sDIC, which, together with measurements of relevant additional physical and chemical parameters, permit us, with a diagnostic model, to quantitatively determine the contribution of all major processes which govern the upper ocean carbon cycle near Station ALOHA.

[42] This ^{13}C-based model is shown schematically in Figure 7. The model includes two oceanic boxes: an upper representing the surface mixed layer and a lower representing the underlying waters of the thermocline. The model also includes an atmospheric box without a prescribed capacity, which provides boundary conditions for the exchange of CO_2 and $^{13}CO_2$ across the air-sea interface. A subsurface boundary between the two oceanic boxes is allowed to move up and down, as prescribed by observations. Lateral transport processes can act as sinks or sources of carbon, depending on prescribed lateral gradients and inferred magnitude and direction of water flow. All tracers are assumed to have uniform concentrations throughout the atmospheric and mixed layer boxes, but concentrations vary linearly with depth in the thermocline box.

[43] The model depicts the following processes: (1) air-sea gas exchange at the sea surface, (2) vertical diffusion across the boundary with the thermocline, (3) entrainment of DIC from the thermocline whenever the mixed layer deepens, (4) horizontal transport, and (5) net community production. The model does not take into account $CaCO_3$ production or dissolution, processes that appear to be unimportant at Station ALOHA as evidenced from the near constancy of sAlk. Mesoscale processes such as eddies are not resolved by the model. Nevertheless, their effects are included implicitly as the observed quantities that form the basis for our diagnostic calculations contain the net effect of these processes.

[44] The model is a modified version of the diagnostic box model described by *Gruber et al.* [1998]. As explained in detail in Appendix C, the main differences consist in the treatment of horizontal transport and how the observed sDIC variations are used as a constraint. *Gruber et al.* [1998] estimated horizontal transport on the basis of independent data and then used the model-simulated temporal evolution of sDIC to evaluate the results with the observed sDIC variations. The benefit of this approach is that one has an independent check, but it causes problems when the model is applied to multiyear records, as the absence of a requirement to match the observed sDIC evolution may lead to substantial misfits over time. Second, very little is known about year-to-year variations in horizontal transport. These problems are lessened if the model equations are solved simultaneously for sDIC and ^{13}C, as this permits estimation of variations in horizontal transport (or any other process in addition to NCP). We therefore adopted this second solution scheme here, as did *Gruber et al.* [2002] for analyzing interannual variability near Bermuda. This latter approach is conceptually analogous to a double deconvolution of atmospheric CO_2 and $\delta^{13}C$ data [*Keeling et al.*, 1989], whereas the method used by *Gruber et al.* [1998] is analogous to a single deconvolution. *Quay and Stutsman* [2003] employed essentially the same double deconvolution method as we do here, except that they estimated horizontal transport and solved for NCP and vertical transport.

[45] For details the reader is referred to Appendix C and *Gruber et al.* [1998]. The results reported here are the climatological mean seasonal cycles diagnosed from these simulations. The model is also used to study interannual

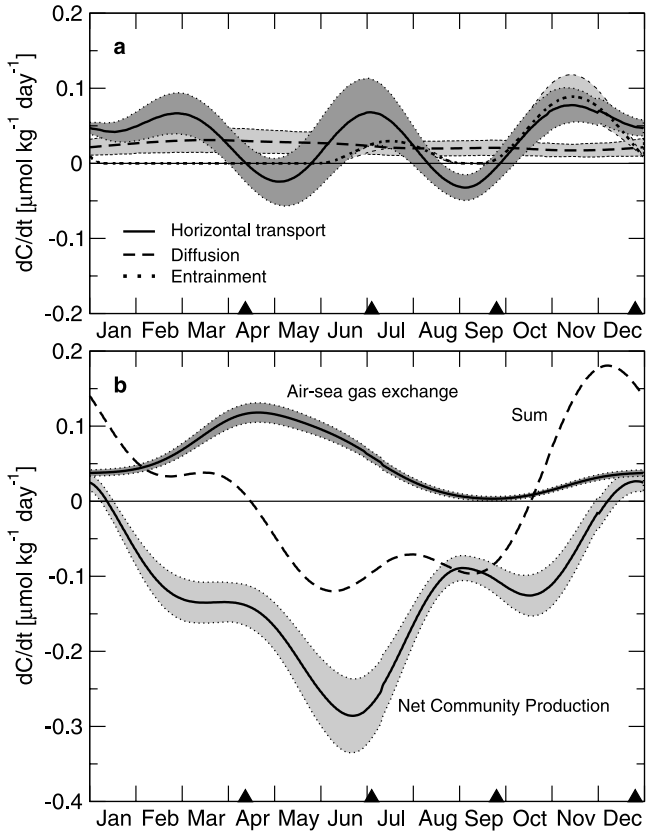

Figure 8. Diagnosed annual cycles for the source terms of sDIC due to (a) horizontal transport, diffusion, and entrainment, and (b) air-sea gas exchange, net community production, and the sum of all five terms (which equals the observed cycle). The different lines denote the computed curves, while the gray shading indicates the uncertainty interval as evaluated from Monte Carlo simulations. The solid triangles denote the four seasons as defined in Tables 3 and 4.

variability, as reported in a companion paper [*Brix et al.*, 2004].

5.3. Seasonal Rates and Fluxes

[46] The mean seasonal cycles of the computed source terms of the five processes considered in the model are displayed in Figure 8. Their standard deviations are derived from Monte Carlo runs.

[47] The source term for vertical diffusion, J_{diff} (see Figure 8a), varies little over the annual cycle, with values between 0.02 and 0.03 μmol kg^{-1} day^{-1}. The entrainment term (J_{ent}) is zero when the base of the mixed layer is shoaling, as occurs between January and May, or stationary, as in August and September. In mid-July, entrainment reaches an intermediate maximum of 0.03 μmol kg^{-1} day^{-1}, but in autumn has its largest influence on the carbon budget of the mixed layer, reaching almost 0.09 μmol kg^{-1} day^{-1} when the deepening of the mixed layer is most intense (Figure 6b) and the vertical DIC gradient at the base of the mixed layer is large (Figure C1a). Estimated uncertainties for J_{ent} are as high as 0.03 μmol kg^{-1} day^{-1}, maximum near when entrainment peaks.

[48] Horizontal transport (J_{htr}, solid line in Figure 8a), as calculated, varies substantially over the annual cycle. From mid-April to May, and again from mid-August to early October, J_{htr} contributes a sink for sDIC. For the remainder of the year, it is a source with a maximum of approximately 0.09 μmol kg^{-1} day^{-1} in late November. All values, however, have to be regarded with caution, as the calculated uncertainties are large (0.02 to 0.06 μmol kg^{-1} day^{-1}).

[49] Air-sea gas exchange (J_{ex}, Figure 8b) provides an almost continuous source of sDIC to the mixed layer. In autumn, J_{ex} rises slowly, when the rapid growth of ΔpCO_2 is partially compensated for by deepening of the mixed layer, in which the DIC flux distributes over a progressively increasing volume. In late winter, J_{ex} accelerates, caused by high ΔpCO_2 and a shoaling of the mixed layer; it peaks in April at about 0.12 μmol kg^{-1} day^{-1}. During spring and summer it decreases owing to a temperature-induced rise in pCO_2. Because the terms determining the air-sea gas exchange are well constrained, J_{ex} is statistically uncertain by only about 0.01 μmol kg^{-1} day^{-1}.

[50] Net community production (NCP), as calculated, is negative most of the year, with maximum negativity in June (-0.28 ± 0.06 μmol kg^{-1} day^{-1}, see Figure 8b). This maximum occurs later than a reported maximum in net primary production (NPP) in late winter and early spring [*Karl et al.*, 1996]. The difference, NPP − NCP, which represents heterotrophic respiration, therefore decreases relative to NPP from winter to summer. A likely cause is shoaling of the mixed layer, although the relative timing needs to be interpreted cautiously given uncertainties in the calculated NCP source term of as much as 0.06 μmol kg^{-1} day^{-1}. Also, a secondary NCP maximum is evident in October, close in time to a secondary NPP peak. The latter peak has been attributed by *Karl et al.* [1996] to enhanced nitrogen fixation by cyanobacteria. We need to emphasize, however, that variations in our results on timescales shorter than about 4 months approach the maximum resolution in our data (sampling interval of 5 to 6 weeks) and can therefore be aliased by our selection of a maximum resolution of 4 months in our harmonic fits. Regardless of these uncertainties, the model clearly demonstrates that NCP, in interaction with air-sea gas exchange and horizontal transport, is the major driver for the seasonal variations in sDIC in the mixed layer at Station ALOHA.

5.4. Mixed Layer Carbon Budgets

[51] To investigate the seasonally changing balance between processes in the mixed layer and the annual averages of processes, we integrate the source terms over each of the four seasons and over the entire year ($\mathcal{J}_i = \int J_i dt$). The four periods (defined in Table 3; black triangles in Figure 8) have been chosen to typify seasonal variability. The values for the standard model run and their associated standard deviations calculated from the Monte Carlo experiments are listed in Table 3.

[52] Over the year, the integrated source term for NCP is calculated to be -45.5 ± 13.2 μmol kg^{-1}; it is primarily compensated by the sum of air-sea gas exchange

Table 3. Temporally Integrated Source Terms, $\mathcal{J}$, as Calculated by the Diagnostic Box Model

Process	Spring,[a] μmol kg^{-1}	Summer,[b] μmol kg^{-1}	Autumn,[c] μmol kg^{-1}	Winter,[d] μmol kg^{-1}	Annual μmol kg^{-1}
			Inferred From Model		
$\mathcal{J}_{ex}$	7.7 ± 0.8	1.4 ± 0.4	1.8 ± 0.3	6.7 ± 0.8	17.7 ± 2.6
$\mathcal{J}_{ncp}$	−17.9 ± 3.7	−12.0 ± 2.6	−6.4 ± 3.3	−8.7 ± 3.6	−45.5 ± 13.2
$\mathcal{J}_{diff}$	2.2 ± 1.2	1.6 ± 0.8	1.6 ± 0.8	2.9 ± 1.6	8.4 ± 4.5
$\mathcal{J}_{ent}$	0.4 ± 0.2	1.1 ± 0.4	5.3 ± 1.9	0.1 ± 0.0	6.9 ± 2.5
$\mathcal{J}_{htr}$	0.9 ± 3.5	1.4 ± 2.5	4.4 ± 3.3	5.6 ± 3.4	12.4 ± 12.9
			Total Inferred From Model		
$\Sigma\mathcal{J}$	−6.8	−6.4	6.6	6.7	0.0

[a]Calendar day 102 to 183.
[b]Calendar day 184 to 264.
[c]Calendar day 265 to 354.
[d]Calendar day 355 to 101.

(17.7 ± 2.6 μmol kg^{-1}) and horizontal transport (12.4 ± 12.9 μmol kg^{-1}). The two remaining terms are of similar source strength: diffusion (8.4 ± 4.5 μmol kg^{-1}) and entrainment (6.9 ± 2.5 μmol kg^{-1}). Similar conclusions are reached by studying the corresponding fluxes into or out of the mixed layer (i.e., the source terms integrated vertically from the base of the mixed layer to the surface, $F_i = \rho_0 h J_i$, with ρ_0 the average density of seawater). Table 4 gives the values for the temporally integrated fluxes $\mathcal{F}_i = \int F_i dt$. Over the annual cycle, air-sea gas exchange adds 0.99 ± 0.13 mol m^{-2}, diffusion and entrainment add approximately the same amount (0.50 ± 0.27 mol m^{-2} and 0.47 ± 0.17 mol m^{-2}, respectively), and horizontal transport adds 0.93 ± 0.78 mol m^{-2}. Over the course of the year, the total of these four additions, 2.89 mol m^{-2}, is substantially offset by NCP removing 2.26 ± 0.80 mol m^{-2}, leaving an annual imbalance of 0.63 mol m^{-2}. This imbalance is due to the covariance between the mixed layer depth and the observed *d*sDIC/*dt*; that is, sDIC in the mixed layer tends to decrease when the depth of the mixed layer is shoaling and vice versa. We therefore require a flux term $\rho_0 \int \mathrm{DIC}\,(dh/dt)dt$ to close the mixed layer budget over the annual cycle.

6. Discussion of Seasonal Results

[53] Taking the seasonal mean results of our model applied to the 14-year CDRG record as a basis, we now address the seasonal drawdown of sDIC in the mixed layer and the persistent oceanic sink for atmospheric CO_2 near Hawaii. Also, we discuss how biological productivity and oceanic transport relate to the inorganic carbon budget observed at Station ALOHA.

6.1. Seasonal Drawdown of Inorganic Carbon

[54] The seasonal drawdown of mixed layer sDIC at Station ALOHA mirrors an increase in sea-surface temperature. *Winn et al.* [1994] attributed this anti-correlation primarily to outgassing of CO_2 during summer caused by surface ocean warming. Our model calculations indicate that this anti-correlation also involves NCP, which shows strong seasonal co-variation with temperature, thus supporting findings of *Quay and Stutsman* [2003].

[55] Quantitatively, the 14-year average spring-summer drawdown of mixed layer sDIC, from 12 April to 21 September of −13.2 μmol kg^{-1}, is caused mainly by NCP, which removes 29.9 μmol kg^{-1}. Gas exchange adds 9.1 μmol kg^{-1}, accompanied by small additions from diffusion, entrainment, and horizontal transport (3.8 μmol kg^{-1}, 1.5 μmol kg^{-1}, and 2.3 μmol kg^{-1}, respectively) (see Table 3). In autumn and winter the oceanic sDIC reservoir is replenished by entrainment (5.4 μmol kg^{-1}), horizontal transport (10.0 μmol kg^{-1}), diffusion (4.5 μmol kg^{-1}), and air-sea gas exchange (8.5 μmol kg^{-1}). Their sum overwhelms the withdrawal of 15.1 μmol kg^{-1} by NCP, causing an increase in sDIC of 13.3 μmol kg^{-1}.

6.2. Oceanic Sink for Atmospheric CO_2

[56] From 1988 to 2002 at Station ALOHA, we estimate a mean annual uptake of CO_2 from the atmosphere of 1.0 ± 0.1 mol C m^{-2} yr^{-1} ($\mathcal{F}_{ex}$, Table 4). In comparison, *Winn et al.* [1994] estimated a net flux of 0.7 mol C m^{-2} yr^{-1} from 1989 to 1992 and *Quay and Stutsman* [2003] estimated 0.6 ± 0.4 mol C m^{-2} yr^{-1} from 1994 to 1999. Our estimated fluxes for these latter respective periods are 0.95 mol C m^{-2} yr^{-1} and 1.10 mol C m^{-2} yr^{-1}, indicating that substantial uncertainties exist in either the chemical data or the flux calculations, or both.

[57] It is instructive to compare these local flux estimates with those obtained for a broad region of the North Pacific Ocean. *Wanninkhof et al.* [2001], on the basis of the ΔpCO_2

Table 4. Integrated Fluxes, $\mathcal{F}$, as Calculated by the Diagnostic Box Model

Process	Spring,[a] mol m^{-2}	Summer,[b] mol m^{-2}	Autumn,[c] mol m^{-2}	Winter,[d] mol m^{-2}	Annual mol m^{-2}
			Inferred From Model		
$\mathcal{F}_{ex}$	0.31 ± 0.03	0.06 ± 0.02	0.14 ± 0.02	0.47 ± 0.05	0.99 ± 0.13
$\mathcal{F}_{ncp}$	−0.72 ± 0.15	−0.57 ± 0.12	−0.39 ± 0.26	−0.56 ± 0.26	−2.26 ± 0.80
$\mathcal{F}_{diff}$	0.09 ± 0.05	0.08 ± 0.04	0.12 ± 0.06	0.22 ± 0.11	0.50 ± 0.27
$\mathcal{F}_{ent}$	0.01 ± 0.01	0.05 ± 0.02	0.39 ± 0.14	0.01 ± 0.00	0.47 ± 0.17
$\mathcal{F}_{htr}$	0.04 ± 0.14	0.06 ± 0.12	0.36 ± 0.25	0.46 ± 0.25	0.93 ± 0.78
			Total Inferred From Model		
$\Sigma\mathcal{F}$	−0.27	−0.31	0.62	0.60	0.63[e]

[a]Calendar day 102 to 183.
[b]Calendar day 184 to 264.
[c]Calendar day 265 to 354.
[d]Calendar day 355 to 101.
[e]This term is balanced over the annual cycle by a covariance term between DIC and *h*, i.e., $\mathcal{F}_{covar} = \rho_0 \int \mathrm{DIC}(dh/dt)dt$.

climatology of *Takahashi et al.* [2002], computed a mean CO_2 uptake of about 0.5 mol C m^{-2} yr^{-1} for the subtropical North Pacific from 13°N to 36°N for a nominal year of 1995. On the basis of an inverse calculation using DIC data from the interior of the ocean, *Gloor et al.* [2003] inferred an uptake of 1.1 mol C m^{-2} yr^{-1} for the same area for a nominal year of 1990.

[58] These estimates indicate a considerable sink for atmospheric CO_2 near Hawaii and for the NPSG as a whole. Before discussing possible mechanisms, it is important to separate the presently observed uptake flux into its natural and anthropogenic components. *Gloor et al.* [2003] estimated the uptake for the subtropical North Pacific to consist of a natural flux of about 0.8 mol C m^{-2} yr^{-1} and an anthropogenic flux of about 0.3 mol C m^{-2} yr^{-1}. The latter flux estimate is somewhat smaller than the global mean anthropogenic CO_2 flux of about 0.5 mol C m^{-2} yr^{-1} (computed by dividing the current consensus global estimate of about 2 Pg Cyr^{-1} from 1980 to 2000 [*Prentice et al.*, 2001] by the total ice-free area of the ocean). Subtropical gyres are expected to have lower than global mean uptake rates of anthropogenic CO_2, because their waters have relatively long residence times near the surface, which permit the waters to adjust to nearly the full anthropogenic CO_2 signal. This point is illustrated by our data, which indicate growth rates of oceanic pCO_2 near Bermuda and Hawaii that are close to or even greater than that of atmospheric pCO_2 (see above and *Gruber et al.* [2002]). This implies that the air-sea pCO_2 difference associated with the anthropogenic CO_2 perturbation is relatively small, leading to a lower than average uptake of anthropogenic CO_2. If we adopt the anthropogenic CO_2 flux estimate of *Gloor et al.* [2003] for the subtropical North Pacific as representative for Station ALOHA, we need to explain an uptake of natural CO_2 of about 0.7 mol C m^{-2} yr^{-1}.

[59] Processes to consider are net heat fluxes, biologically induced changes in DIC and Alk, and the interaction of these two with large-scale ocean circulation [*Gruber and Sarmiento*, 2002]. We can neglect the impact of freshwater fluxes for the climatological mean CO_2 flux that we consider here, although we have seen above that changes in the freshwater balance of the upper ocean can lead to substantial changes in the air-sea CO_2 fluxes.

[60] Net air-sea heat fluxes around Hawaii appear to be near zero [*Esbensen and Kushnir*, 1981; *Kalnay et al.*, 1996]. However, owing to the long time it takes for surface ocean DIC to equilibrate with atmospheric CO_2 after SST has been perturbed by a net air-sea heat flux [*Broecker and Peng*, 1974], thermally induced air-sea fluxes of CO_2 can persist for a year of more after the initial heat flux forcing has subsided. Our diagnostic modeling result tends to suggest that horizontal transport brings surface waters from the northeast to Station ALOHA. Existing heat flux climatologies suggest that these waters have undergone cooling before arriving at Station ALOHA, so that at least a part of the net CO_2 uptake from the atmosphere at Station ALOHA is probably driven by net cooling. This thermally driven CO_2 flux is not due to local heat fluxes, but rather to a negative heat flux upstream, whose impact is carried downstream because of the slow air-sea CO_2 gas exchange. However, given the relatively sluggish circulation, we suspect that this thermally induced CO_2 uptake explains only a small fraction of the net CO_2 uptake of about 0.7 mol C m^{-2} yr^{-1}.

[61] With physical mechanisms apparently inadequate to explain the entire oceanic CO_2 sink near Hawaii, biological processes in connection with large-scale circulation must play an important role as well. We can exclude any biological process associated with Alk, as Alk behaves nearly conservatively in the subtropical North Pacific [see also *Millero et al.*, 1998]. In contrast, our diagnostic modeling calculations indicate a substantial impact of ocean biology on sDIC. However, our diagnosed NCP of 2.3 mol C m^{-2} yr^{-1} for the mixed layer does not automatically imply a biologically induced uptake of CO_2 from the atmosphere. The net impact of biological processes on the exchange of CO_2 between the ocean and atmosphere depends on the balance between upward supply of remineralization derived high DIC waters and the net fixation of this DIC into organic matter and downward export [*Gruber and Sarmiento*, 2002]. Regions, where the upward and lateral supply of high DIC waters accompanied by high nutrient concentrations exceeds local net biological export, develop a biologically induced CO_2 supersaturation tendency and hence lose CO_2 to the atmosphere. In contrast, regions where net biological fixation of CO_2 exceeds the local vertical and lateral supply of DIC tend to take up CO_2 from the atmosphere. We postulate that the region near Hawaii belongs to the latter category, and that a substantial fraction of the net CO_2 uptake, which we estimated on the basis of our data, is of local biological origin. This conclusion is supported by our finding that NCP at Station ALOHA exceeds the total physical supply of inorganic carbon stemming from horizontal transport, vertical entrainment, and vertical diffusion.

[62] *Winn et al.* [1994] similarly argued for a biologically induced CO_2 sink at Station ALOHA. However, they suggested that this sink is not produced locally, but is primarily a result of an Ekman drift induced advection of waters from the eastern and tropical Pacific Ocean, where biologically induced outgassing of CO_2 has led to a DIC deficit that is replenished slowly as these waters move northward. Our diagnostic model calculations support a modification of their hypothesis, as we find net horizontal flow to come from northerly rather than southerly direction.

[63] Our interpretation that a substantial fraction of the net uptake of CO_2 at Station ALOHA is driven by local biological processes requires the region around Station ALOHA to be also a net sink for bio-utilizable inorganic nutrients. How could these nutrients be supplied? We offer two possibilities.

[64] One of these is that transport, either horizontal or vertical, supplies nutrients at such ratios to inorganic carbon that surface waters become undersaturated relative to atmospheric CO_2 after all nutrients have been taken up. Thermocline waters of many regions of the world oceans, indeed, have a potential for taking up CO_2 from the atmosphere, most likely driven by the slowness of air-sea exchange which fails to equilibrate surface waters with the atmosphere where thermocline waters are formed [*Gruber*

Table 5. Comparison of Estimates of Net Community Production and Export Production in the Subtropical North Pacific

Reference	Type of Production[a]	Estimate[b]	Time	Depth Range	Method
Emerson et al. [1997]	NCP	2.7 ± 1.7	1990, 1992, 1995	upper 100 m	O_2, Ar, N_2 mass balance
	NCP	1.6 ± 0.9	1990, 1994	upper 100 m	DI^{13}C mass balance
	NCP	2.0 ± 0.9	1990, 1992, 1995	upper 100 m	Σ organic carbon fluxes
Sonnerup et al. [1999]	NCP	2.2 ± 0.5	1991	export at 100 m	CFC based model
	NCP	1.5 ± 0.3	1991	export at 150 m	CFC based model
Benitez-Nelson et al. [2001]	total C flux	2.7 ± 0.9	1988–1999	upper 150 m	^{234}Th based
	POC flux	1.5 ± 0.8	1999–2000	upper 150 m	^{234}Th based
Karl et al. [1995]	POC flux	0.9 ± 0.3	1989–1992	export at 150 m	sediment traps
Neuer et al. [2002]	POC flux	1.0 ± 0.2	1996–1998	export at 150 m	sediment traps
Quay and Stutsman [2003]	NCP	2.6 ± 1.3	1994–1999	mixed layer	diagn. ML model
This study	NCP	2.3 ± 0.8	1988–2002	mixed layer	diagn. ML model

[a]POC: particulate organic carbon.
[b]Units are mol C $m^{-2}yr^{-1}$.

and Sarmiento, 2002]. A second possibility is that nutrient sources not associated with inorganic carbon sources are involved, such as atmospheric deposition, or in situ N_2 fixation. While the atmospheric deposition of nutrients is reported to be low near Station ALOHA [*Duce et al.*, 1991], *Karl et al.* [1997] estimated that N_2 fixation at Station ALOHA adds annually 31 to 51 mmol N m^{-2} yr^{-1} to the mixed layer, consistent with a basin-wide estimate by *Deutsch et al.* [2001]. Assuming that N_2 fixation typically occurs at a C:N ratio of 10:1 [*Karl et al.*, 2002], this annual N_2 fixation could promote a conversion of dissolved inorganic to organic carbon of 0.31 to 0.51 mol C m^{-2} yr^{-1}. In the extreme case that all of this nitrogen-supported organic carbon, originally supplied from the atmosphere, were exported to deeper water, N_2 fixation would account for more than half of the observed sink for natural CO_2. Such a N_2 fixation-based proposal raises the question, however, as to how the required phosphorus is supplied. Possible mechanisms include horizontal transport of dissolved organic phosphorus [*Abell et al.*, 2000; *Emerson et al.*, 2001] and vertical migration [*Villareal et al.*, 1999; *Karl et al.*, 1997]. We will return to this issue below. In summary, we propose that the oceanic region near Hawaii is a sink for natural CO_2 from the atmosphere mainly because of net biological fixation and export locally exceeding the vertical and lateral supply of inorganic carbon, rather than the transport of *DIC* poor waters from the tropical Pacific, as suggested by *Winn et al.* [1994].

6.3. Biological Production

[65] The diagnostic model-based estimate of NCP for the mixed layer of 2.3 ± 0.8 mol C m^{-2} yr^{-1} is compared in Table 5 to estimates from other studies for Station ALOHA. These studies differ among themselves not only by the methods used, but also because NCP is not necessarily equivalent to several of the other estimates of carbon export. Depth ranges also differ, and a direct comparison of the results neglects possible interannual variability.

[66] To achieve a better comparison, we extrapolate our results to the entire euphotic zone, whose base has been determined to be 173 ± 7 m [*Karl et al.*, 1996]. Measurements of NPP show that roughly 80% of NPP takes place within the mixed layer [*Lukas and Karl*, 1999]. Assuming that the depth dependence of NCP scales with the depth dependence of NPP, we estimate NCP for the entire euphotic zone to be approximately 2.8 mol C m^{-2} yr^{-1} (2.3 mol C m^{-2} yr^{-1} divided by 0.8). If we further assume an approximate steady state for the carbon cycle at Station ALOHA over the annual cycle, it follows that NCP is numerically equivalent to various estimates of export production, listed in Table 5. *Emerson et al.* [1997], using results obtained by three independent experimental approaches, carried out mass balance calculations that yielded export fluxes between 1.6 ± 0.9 and 2.7 ± 1.7 mol C m^{-2} yr^{-1} in the upper 100 m. *Sonnerup et al.* [1999], from estimates of oxygen utilization rates based on chlorofluorocarbons (CFCs), found 2.2 ± 0.5 mol C m^{-2} yr^{-1} at 30N, 152W. From ^{234}Th based export estimates, *Benitez-Nelson et al.* [2001] found 2.7 ± 0.9 mol C m^{-2} yr^{-1} in the upper 150 m at Station ALOHA. *Quay and Stutsman* [2003] found 2.6 ± 1.3 mol C m^{-2} yr^{-1} for just the mixed layer at Station ALOHA, derived from a ^{13}C based diagnostic mixed layer model. Our estimate for NCP is thus similar to previous estimates obtained with a variety of methods, but perhaps in the upper range.

6.4. Horizontal Versus Vertical Supply

[67] While our estimates for NCP and air-sea exchange are similar to those obtained by *Quay and Stutsman* [2003], and our approach is similar, we disagree on the relative importance of horizontal and vertical pathways of supply of DIC to the mixed layer. Over the annual cycle, we find that horizontal transport (0.9 ± 0.8 mol m^{-2} yr^{-1}) is a substantial part of the supply of inorganic carbon afterward removed by NCP (2.3 ± 0.8 mol m^{-2} yr^{-1}). Thus this transport is about equal to vertical transport, which is the sum of vertical diffusion (0.5 ± 0.3 mol m^{-2} yr^{-1}) and entrainment (0.5 ± 0.2 mol m^{-2} yr^{-1}). In contrast, *Quay and Stutsman* [2003] find that horizontal transport produces an annual DIC sink of 0.4 ± 0.3 mol m^{-2} yr^{-1}, while vertical transport supplies 2.4 ± 1.2 mol m^{-2} yr^{-1}.

[68] These large disagreements reflect differing modeling approaches. *Quay and Stutsman* [2003] assumed that horizontal transport is better known than vertical transport, and set up their equations to solve for the latter term together with NCP. They calculated the contribution of horizontal transport to the mixed layer sDIC budget from independent estimates of the horizontal sDIC gradient and of the mean horizontal flow. The latter they determined by combining an estimate of the mean Ekman transport derived from wind data (0.021 m s^{-1} northward and 0.004 m s^{-1} westward) with an estimate of the geostrophic flow derived

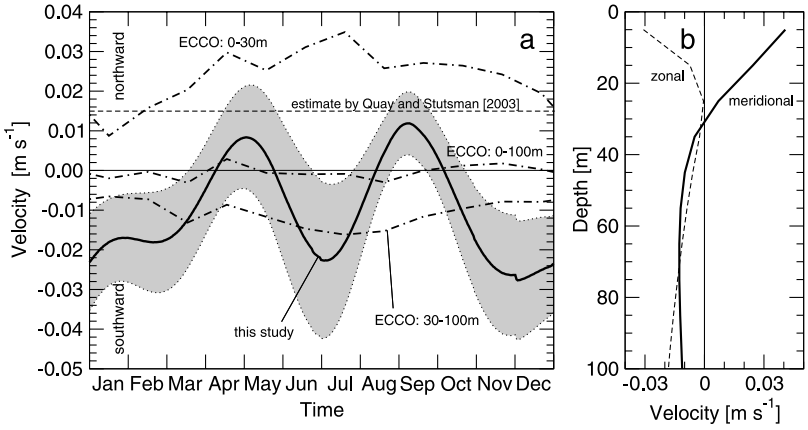

Figure 9. Meridional velocities of upper ocean currents near Station ALOHA. (a) Plot of seasonal variations of the meridional velocity estimated by different studies. Shown as a solid black line are our estimates inferred from the diagnostic box model with the grey bands indicating the uncertainty estimated from the Monte Carlo simulations. The estimate used by *Quay and Stutsman* [2003] is shown as a dashed line. Also shown as dash-dotted lines are the upper ocean currents estimated by the ECCO reanalysis model [*Stammer et al.*, 2002], averaged over different depth intervals. (b) Vertical profiles of the meridional (solid line) and zonal (dashed line) velocities estimated by the ECCO reanalysis model.

from climatological hydrographic data (0.006 m s^{-1} southward and 0.011 m s^{-1} eastward), therefore resulting in total horizontal velocities of 0.015 m s^{-1} northward and 0.007 m s^{-1} eastward. Alternatively, we have regarded the processes controlling vertical transport to be known better than those controlling horizontal transport, and have solved the diagnostic equations for the latter, together with NCP; that is, we have estimated the vertical diffusivity at the base of the mixed layer on the basis of the vertical stability of the water column there (see Appendix C) and then diagnosed horizontal velocities which satisfy the carbon budget.

[69] Since both *Quay and Stutsman* [2003] and we used similar estimates of horizontal and vertical gradients, the two approaches must differ mainly in their estimates of vertical diffusivity and horizontal advective velocities. In Figure 9a, our meridional velocity estimates, inferred from the carbon budget at Station ALOHA, are compared to that of *Quay and Stutsman* [2003]. We focus here only on the meridional transport, since zonal transport is much smaller, owing to a much smaller zonal gradient of sDIC. Our inferred horizontal velocities indicate that the annual mean flow is directed southward with a velocity of about 0.012 m s^{-1}, compared with the northward mean velocity of 0.015 m s^{-1} assumed by *Quay and Stutsman* [2003]. Our results also suggest substantial seasonal variations, with southward transport in November through February and northward transport in April/May and late August/September. However, we have little confidence in the model estimates of these subseasonal variations. A first reason is that we assumed horizontal gradients to be constant over the annual cycle, which is quite likely not the case. Second, as pointed out above, our observations have a resolution of only about 4 to 5 weeks, which makes the interpretation of seasonal trends on timescales shorter than a few months tenuous.

[70] In order to assess our results and possibly discriminate between the two views about the dominant pathways of inorganic carbon (and nutrient) supply to the upper ocean near Station ALOHA, we extracted the meridional and zonal velocities in the vicinity from the reanalysis model of the "Estimating the Circulation and Climate of the Ocean" (ECCO) project [*Stammer et al.*, 2002] (data available from http://www.ecco-group.org). This model estimates the state of the ocean circulation that is optimally consistent with oceanic observations, such as sea-surface height, temperatures, and salinities. We extracted the data from a model version that uses the adjoint technique to assimilate these observations, generally considered to produce the most accurate solutions [*Stammer et al.*, 2002]. Figure 10a shows the annual mean velocities averaged over the top 100 m. The respective contributions to this average from the surface down to 30 m and from 30 m to 100 m are shown in Figures 10b and 10c, respectively. This analysis reveals that while the zonal flow in the region around Station ALOHA comes from the east independent of depth, the meridional flow shows a strong baroclinic component. In the upper 30 m, the meridional flow is northward, with velocities exceeding 0.03 m s^{-1}, while below that depth, the meridional flow is southward, with velocities between 0.01 and 0.02 m s^{-1} (see depth profile in Figure 9b). This baroclinicity is the result of a superposition of a surface-intensified Ekman transport from the southeast, and a nearly barotropic geostrophic transport from the northeast. Figure 9a compares the meridional velocities estimated by ECCO for the nearest grid point to Station ALOHA with our estimates and those obtained by *Quay and Stutsman* [2003]. Zonal velocities are not shown, but we note that *Quay and Stutsman* [2003] estimated them to be directed eastward, opposite of what we expect and of what ECCO estimates.

[71] The comparison of the meridional velocities reveals that it is not straightforward to assess whether the meridional velocity estimated by *Quay and Stutsman* [2003] is more or less correct than ours, as this depends strongly on the assumptions being made about the depths over which

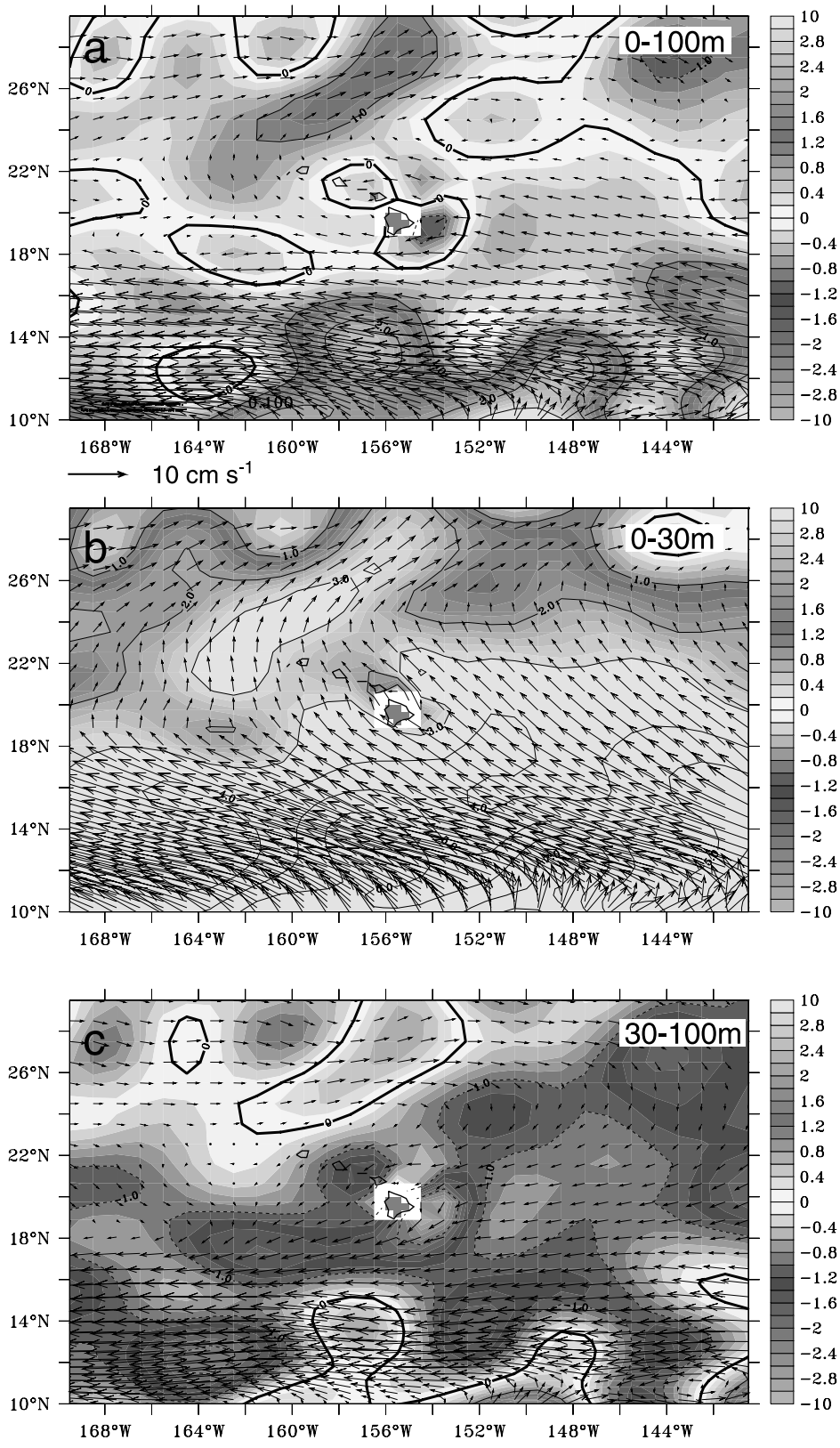

Figure 10. Maps of upper ocean circulation in the vicinity of Hawaii estimated by the ECCO reanalysis model [*Stammer et al.*, 2002]. (a) 0–100 m averages, (b) 0–30 m averages, and (c) 30–100 m averages. The vectors show the total velocity, while the contours show the magnitude of the meridional velocity component. Results are the annual averages for the 1997 to 2002 period as simulated by the adjoint version of the ECCO model. Units are cm s^{-1}. See color version of this figure at back of this issue.

the horizontal transport needs to be integrated. *Quay and Stutsman* [2003] calculated their horizontal velocities for the upper 50 m. Their estimate of 0.015 m s^{-1} northward is about twice as large as the ECCO estimate of 0.008 m s^{-1} northward over the same depth region. However, the mean mixed layer depth is about 62 m (see Table 1). Integration of the ECCO velocities over this depth range gives 0.005 m s^{-1} northward. If the relevant flow for the mixed layer budget occurred over the top 100 m, the average meridional velocity would be zero. Given the strong depth dependence of the meridional flow, one needs to take into consideration also the possible depth dependence of the meridional gradients of sDIC and $\delta^{13}C$. For example, if the meridional sDIC gradients at depth are stronger than those at the surface as suggested by a preliminary inspection of the sDIC data, the meridional component of the depth integrated DIC transport likely would come out of the north, consistent with our estimates. However, a much more careful analysis needs to be conducted, which includes consideration of the seasonalities of the mixed-layer depth, of upper ocean transport, and of the horizontal gradients. As we currently lack good seasonal information about the horizontal gradients, this is beyond the scope of this study.

[72] It may turn out that we have overestimated horizontal transport from the north because we may have underestimated vertical diffusion by relying on diffusivity estimates that agree well with those for the mid-thermocline [*Ledwell et al.*, 1993, 1998] but may be too small for waters directly underneath the mixed layer. Possible processes that could lead to enhanced vertical diffusivities in this layer include transient events, such as the passage of storms [*Large et al.*, 1986], breaking of internal waves [*Denman and Gargett*, 1995], and mesoscale variability [*Letelier et al.*, 2000].

[73] We conclude that the presently available data are insufficient to discriminate clearly between the two views about the dominant pathways of inorganic carbon (and nutrient) supply to the upper ocean near Station ALOHA, although both studies agree on the likelihood that lateral processes are important in controlling the upper ocean carbon cycle near Station ALOHA. We point out that a near-surface northward flow would tend to supply DOP to the region around Station ALOHA, as DOP concentrations increase equatorward of Hawaii [*Abell et al.*, 2000; *Emerson et al.*, 2001]. This could provide the phosphorus source needed to support the elevated rates of N_2 fixation at Station ALOHA [*Karl et al.*, 1997] and hence ultimately contribute to the biologically mediated CO_2 uptake from the atmosphere. This argument remains tentative without long-term in situ measurements of horizontal velocities and vertical mixing, needed to discriminate between the two views.

7. Comparison With Bermuda: Carbon Cycling in the Subtropical Gyres

[74] To put our results from Station ALOHA into a broader context, we now make a comparison with prior results from the North Atlantic subtropical gyre at the Station "S"/Bermuda Atlantic Time series Site (BATS) near Bermuda [*Gruber et al.*, 1998, 2002], the only other oceanic site having a similar chemical record.

[75] The average sDIC trend observed for Station ALOHA, 1.22 ± 0.08 μmol kg^{-1} yr^{-1} from 1988 to 2002, is substantially greater than the trend of 0.64 ± 0.05 μmol kg^{-1} yr^{-1} observed for Station "S"/BATS from 1983 to 2001 (see Table 1). Similarly, the oceanic pCO_2 trend observed for Station ALOHA is 2.5 ± 0.1 μatm yr^{-1}, substantially greater than 1.5 ± 0.1 μatm yr^{-1} observed for Station "S"/BATS. The latter trend is close to the atmospheric trend, suggesting a lack of natural decadal variability and regime shifts near Bermuda in comparison to evidence of such variability at Station ALOHA.

[76] In contrast to the comparison for sDIC, the average decrease in $\delta^{13}C^{oc}$ observed at Station ALOHA (−0.027 ± 0.001‰ yr^{-1}) is similar to that near Bermuda (−0.024 ± 0.001‰ yr^{-1}). This difference in trends in $\delta^{13}C^{oc}$ and sDIC is likely to be owing to the smaller horizontal gradients in $\delta^{13}C^{oc}$ compared to DIC, which makes the $\delta^{13}C^{oc}$ trends insensitive to changes in salinity, and also to the relatively long equilibration timescale for air-sea exchange of isotopic DIC compared to DIC.

[77] A comparison of the seasonal carbon cycle of the upper ocean at Station ALOHA with that for Station "S"/BATS [*Bates et al.*, 1996; *Gruber et al.*, 1998; *Bates*, 2001] shows both similarities and differences. While the phasing for sDIC and $\delta^{13}C^{oc}$ are nearly the same at both locations, the observed amplitudes at Station ALOHA (15 μmol kg^{-1} and 0.09‰, respectively) are only about half of those at Station "S"/BATS (32 μmol kg^{-1} and 0.20‰). With regard to seasonally varying pCO_2, the almost year-round CO_2 undersaturation at Station ALOHA contrasts with alternating undersaturation and supersaturation at BATS. The seasonal patterns for the mixed layer depth are similar for both stations, but again the amplitudes are much less pronounced at Station ALOHA.

[78] One might argue that the primary reason for these differences is the much more vigorous seasonal cycle of mixed layer depth near Bermuda, where winter mixed layer depths can exceed 200 m [*Michaels and Knap*, 1996; *Gruber et al.*, 1998]. It turns out, however, that this difference is only of indirect importance, as evidenced by a comparison of the processes that determine the seasonal dynamics of the carbon cycle at these sites according to our diagnostic box-model calculations. Annual NCP calculated for Station ALOHA (−2.3 ± 0.8 mol C m^{-2} yr^{-1}) is about two thirds of that for Station "S"/BATS (−3.4 ± 0.8 mol C m^{-2} yr^{-1}) [*Gruber et al.*, 2002]. Given this result and the similar ratio for annual uptake of atmospheric CO_2, the much smaller seasonal amplitudes for Station ALOHA compared to Station "S"/BATS is at first surprising, but explained by the large difference in seasonally varying chemical behavior for the two sites. Near Bermuda, seasonal variations in air-sea gas exchange and NCP tend to reinforce each other to create a substantial *DIC* loss in the summer season, whereas air-sea exchange tends to oppose NCP at Station ALOHA.

[79] Another notable site difference exists with respect to which biogeochemical and physical processes are most responsible for the annual net uptakes of CO_2 from the atmosphere (1.9 ± 0.2 mol C m^{-2} yr^{-1} for Bermuda versus 1.0 ± 0.1 mol C m^{-2} yr^{-1} for Hawaii). According to

Follows et al. [1996] and *Gruber et al.* [1998], net cooling, by horizontal advection and subduction processes, governs the uptake of natural CO_2 from the atmosphere near Bermuda, whereas near Hawaii we argue for a substantial role to be played by biological processes.

[80] In summary, both sites show dynamic carbon cycles in the upper ocean of the subtropical gyres, with substantial temporal variability, both seasonal and decadal. Although this oceanic carbon variability makes it difficult to identify the long-term accumulation of anthropogenic CO_2, which was originally among the primary reasons for establishing these two time series, this variability provides insight into how the natural carbon cycle responds to natural ecological and biogeochemical changes.

8. Summary and Conclusions

[81] From data sets of physical and biogeochemical quantities measured in the near-surface oceanic mixed layer at Station ALOHA from 1988 through 2002, we find an interplay of local and large-scale biological and physical processes. These we have interpreted with a diagnostic box model of the upper ocean carbon cycle. This model is constrained by concurrent observations of sDIC and $\delta^{13}C^{oc}$ and quantitatively accounts for the five processes that we have identified to govern the carbon cycle there: exchange of CO_2 across the air-sea interface, net community production (NCP) of organic carbon, and transport of inorganic carbon within the upper ocean by horizontal transport, by vertical diffusion, and by vertical entrainment when the mixed layer deepens seasonally.

[82] Focusing on seasonal cycling in this article, we find NCP to be the dominant process causing sDIC to decrease from spring to summer, with an annual integral over the surface mixed layer of 2.3 ± 0.8 mol C m^{-2} yr^{-1}. An extrapolation to the entire euphotic zone yields an annual estimate of about 2.8 mol C m^{-2} yr^{-1}, which, assuming steady state over the annual cycle, can be directly compared with previously published estimates of annual export production. This comparison suggests that our calculated export production is within the range of these published estimates, but toward the high side. A substantial fraction of the inorganic carbon removed from the mixed layer by NCP over the annual cycle is replenished by horizontal transport, with vertical transport by diffusion and entrainment supplying most of the remaining.

[83] The nearly continuous undersaturation of oceanic pCO_2 at Station ALOHA, inferred from our measurements, shows waters at this site to be a persistent sink for atmospheric CO_2, with an annual net flux of 1.0 ± 0.1 mol C m^{-2} yr^{-1}. About 0.3 mol C m^{-2} yr^{-1} of this flux is driven by the uptake of anthropogenic CO_2 from the atmosphere. We argue that the remainder, a natural flux of about 0.7 mol C m^{-2} yr^{-1}, is a consequence of two effects. The first is the cooling of waters upstream of Station ALOHA, whose effect is carried downstream as a result of the relatively slow air-sea gas exchange of CO_2. The second is that net biological fixation of CO_2 in the waters surrounding Station ALOHA and the subsequent export of this fixed organic matter tends to exceed the total vertical supply of inorganic carbon, creating a biologically induced tendency for CO_2 uptake from the atmosphere.

[84] A strong motivation for carrying out this study, and a companion study in the North Atlantic near Bermuda, has been to establish the response of the subtropical ocean water to the rise in atmospheric CO_2 concentrations caused by the release of CO_2 to the air from combustion of fossil fuels and land use change. With 14 years of data gathered for DIC in subtropical waters near Hawaii, and 19 years near Bermuda, it is evident that the surface waters in the subtropical gyres have persistently absorbed this anthropogenic CO_2 at such rates that their surface sDIC concentrations have followed an upward trend at least as large as expected from complete equilibration of the surface ocean CO_2 system with the atmospheric CO_2 perturbation. Near Hawaii, the time series of DIC and oceanic pCO_2 show trends that actually exceed those expected from the uptake of anthropogenic CO_2 from the atmosphere. These high average trends appear to be a result of a marked increase in mixed layer salinity, which occurred around 1997, perhaps related to a large-scale reorganization of the climate system over the North Pacific. In contrast, the long-term mean rate of decrease of $\delta^{13}C^{oc}$ near Hawaii is very close to that expected from the uptake of isotopically depleted anthropogenic CO_2 from the atmosphere, highlighting a unique character for this tracer. Given the unpredictable future behavior of the subtropical ocean carbon cycle, the continuation of this time series, and that near Bermuda, is crucial in understanding the further evolution of the upper ocean carbon cycle and its response to future variability and change.

Appendix A: Measurement Techniques

[85] Duplicate samples of seawater were collected following the procedures described by *Lueker* [1998]. The bottles were shipped to the laboratory of the Carbon Dioxide Research Group (CDRG) of the Scripps Institution of Oceanography, where they were stored in the dark until analysis. Measurement procedures for dissolved inorganic carbon and total titration alkalinity (Alk) are given in detail by *Lueker* [1998] and for the $^{13}C/^{12}C$ ratio of DIC as described below. Salinity, nitrate, phosphate, and silicate were measured on each water sample by the Ocean Data Facility of SIO.

[86] DIC was measured by a cryogenic vacuum extraction followed by a manometric determination of the amount of evolved CO_2 gas. The imprecision of replicate determinations of DIC in the laboratory is about ±0.5 μmol kg^{-1}. The inaccuracy is estimated to be about ±1.0 μmol kg^{-1}. Alk was determined using a closed cell titration through the sampling date of 4 June 1997. The estimated imprecision from replicate determinations is ±1.0 μmol kg^{-1} with an inaccuracy of about ±5 μmol kg^{-1}. Beginning with the sampling date of 9 July 1997, Alk was determined using an open cell titration in the laboratory of Andrew Dickson at SIO, with an imprecision from replicate measurements of ±0.7 μmol kg^{-1} and an inaccuracy estimated to be less than 2 μmol kg^{-1}. The data, as reported, include a false contribution of approximately 0.5 μmol kg^{-1}, because the water samples contained elevated silicic acid concentrations caused by storage in the glass bottles. The CO_2 partial

pressure of seawater was calculated as described in a technical report [*DOE*, 1994], taking into account the contribution to the total alkalinity of nutrient concentrations in the samples. Thus the effect of silicic acid, whether elevated by storage or not, was removed when calculating the CO_2 partial pressure. The $^{13}C/^{12}C$ ratio of DIC was determined on the same extracted CO_2 gas as used for the manometric measurement of DIC. After the manometric measurement, the CO_2 gas was quantitatively collected cryogenically and sealed by flame in glass tubes. Samples taken at Station ALOHA up to December 1990 were shipped to the Centre for Isotope Physics (CIO) of Groningen University, where mass spectrometric analysis of the $^{13}C/^{12}C$ ratio was carried out using a VG SIRA 9 isotope ratio mass spectrometer. Daily calibrations were based on a suite of carbonate and pure CO_2 standards [*Roeloffzen*, 1993]. These standards were repeatedly calibrated against primary standards from the National Bureau of Standards (NBS-18, NBS-19, and VSMOW). An N_2O correction was applied to atmospheric CO_2 samples, none to seawater samples. Samples taken at Station ALOHA from January 1991 to 20 October 1996 were analyzed at the Isotope Laboratory of the Scripps Institution of Oceanography using a VG Prism II isotope mass spectrometer. Samples taken from 30 October 1996 onward were analyzed in the CDRG laboratory using its Micro Mass Optima mass spectrometer. Daily calibrations, based on six secondary standards, were applied to all data, as described by *Bollenbacher et al.* [1998]. Of the six secondary standards, three were prepared at SIO by extracting CO_2 from air stored under high pressure in steel cylinders, two were supplied by CIO of Groningen University (GS19 and GS20), and one was prepared from sodium bicarbonate at SIO. All standards were calibrated against primary standards of CO_2 derived from international isotopic standards of the National Bureau of Standards (NBS-16, NBS-17, and NBS-19).

[87] The effect of changes in analysis procedures and instrumentation between CIO and SIO was examined by analyzing samples of three sodium bicarbonate solution standards and a set of samples extracted from surface seawater collected off southern California [*Bollenbacher et al.*, 1998]. On average, the SIO measurements were greater by 0.016‰ than measurements made at CIO, a difference too small to justify applying an adjustment. The imprecision and estimated inaccuracy of the $\delta^{13}C^{oc}$ analyses are ±0.02‰ and ±0.05‰, respectively.

Appendix B: Total Derivative of DIC

[88] The concentration of DIC is a function of temperature (T), salinity (S), total alkalinity (Alk), and oceanic pCO_2, i.e., DIC = $f(T, S, \mathrm{Alk}, pCO_2^{oc})$. The total derivative of DIC with respect to changes of these quantities is therefore

$$\Delta DIC = \frac{\partial \mathrm{DIC}}{\partial T}\Delta T + \frac{\partial \mathrm{DIC}}{\partial S}\Delta S + \frac{\partial \mathrm{DIC}}{\partial \mathrm{Alk}}\Delta \mathrm{Alk} + \frac{\partial \mathrm{DIC}}{\partial pCO_2^{oc}}\Delta pCO_2^{oc}. \tag{B1}$$

[89] To account separately for stoichiometric changes in Alk (proportional to (AlK = S/S_0 sAlk) and changes owing to freshwater fluxes, we modify the third right-hand term to read

$$\frac{\partial \mathrm{DIC}}{\partial \mathrm{Alk}}\Delta \mathrm{Alk} = \frac{\partial \mathrm{DIC}}{\partial (S/S_0\ \mathrm{sAlk})}\Delta (S/S_0\ \mathrm{sAlk}) = \frac{\mathrm{sAlk}}{S_0}\frac{\partial \mathrm{DIC}}{\partial \mathrm{Alk}}\Delta S + \frac{S}{S_0}\frac{\partial \mathrm{DIC}}{\partial \mathrm{Alk}}\Delta \mathrm{sAlk}. \tag{B2}$$

[90] To separate changes in oceanic pCO_2, driven by changing atmospheric CO_2, from changes caused within the water column, we write

$$\frac{\partial \mathrm{DIC}}{\partial pCO_2^{oc}}\Delta pCO_2^{oc} = \frac{\partial \mathrm{DIC}}{\partial pCO_2^{oc}}\Delta\left(pCO_2^{atm} - \Delta pCO_2\right) = \frac{\partial \mathrm{DIC}}{\partial pCO_2^{oc}}\Delta pCO_2^{atm} - \frac{\partial \mathrm{DIC}}{\partial pCO_2^{oc}}\Delta\Delta pCO_2. \tag{B3}$$

[91] Inserting equations (B3) and (B2) into equation (B1) yields the total derivative of DIC as used in equation (2),

$$\Delta \mathrm{DIC} = \frac{\partial \mathrm{DIC}}{\partial T}\Delta T + \frac{\partial \mathrm{DIC}}{\partial S}\Delta S + \frac{\mathrm{sAlk}}{S_0}\frac{\partial \mathrm{DIC}}{\partial \mathrm{Alk}}\Delta S + \frac{S}{S_0}\frac{\partial \mathrm{DIC}}{\partial \mathrm{Alk}}\Delta \mathrm{sAlk} + \frac{\partial \mathrm{DIC}}{\partial pCO_2^{oc}}\Delta pCO_2^{atm} - \frac{\partial \mathrm{DIC}}{\partial pCO_2^{oc}}\Delta\left(pCO_2^{atm} - pCO_2^{oc}\right). \tag{B4}$$

Appendix C: Diagnostic Model Description

C1. Model Equations

[92] The basic model equations for the concentrations of DIC and of ^{13}C are, respectively,

$$\frac{d\mathrm{DIC}}{dt} = J_{ex} + J_{diff} + J_{ent} + J_{htr} + J_{ncp} \tag{C1}$$

$$\frac{d^{13}\mathrm{C}}{dt} = {}^{13}J_{ex} + {}^{13}J_{diff} + {}^{13}J_{ent} + {}^{13}J_{htr} + {}^{13}J_{ncp}, \tag{C2}$$

where the source terms for DIC are denoted as follows: J_{ex} for air-sea gas exchange, J_{diff} for diffusion, J_{ent} for entrainment, J_{htr} for horizontal transport, and J_{ncp} for the source term due to NCP. The $^{13}J_i$-terms indicate the respective source terms for ^{13}C.

[93] The term, J_{ncp}, for DIC is related to the corresponding ^{13}C source term ($^{13}J_{ncp}$) by the $^{13}C/^{12}C$ ratio of organic matter $^{13}r_{org}$,

$$J_{ncp} = \frac{1 + {}^{13}r_{org}}{{}^{13}r_{org}}\ {}^{13}J_{ncp}. \tag{C3}$$

A similar relationship exists for the horizontal transport,

$$J_{htr} = \frac{1 + {}^{13}r_{grad}}{{}^{13}r_{grad}}\ {}^{13}J_{htr}, \tag{C4}$$

Table C1. Definition of Input Variables of the Diagnostic Box Model

Variable	Unit	Description	Source[a]
sDIC	μmol kg^{-1}	observed sDIC concentration	this study, CDRG
T	°C	mixed layer temperature	HOT program, [1]
S		mixed layer salinity[b]	HOT program, [1]
h	m	mixed layer depth	calc. from T and S, see text
$fCO_2^{oc\ c}$	μatm	oceanic fCO_2	calc. from Alk and DIC, see text
$fCO_2^{atm\ c}$	μatm	atmospheric fCO_2	calc. from xCO_2^{atm}, see text
ws	m s^{-1}	wind speed	NCEP reanalysis, [2]
k	m s^{-1}	gas exchange velocity	calc. from obs. ws, T and S, see text
L	μmol kg^{-1} μatm^{-1}	CO_2 solubility in seawater	calc. from obs. T and S, see text
dDIC/dz $\vert_{tc}$	μmol kg^{-1} m^{-1}	vertical DIC gradient	estimated from HOT DIC data, [1]
dDI^{13}C/dz $\vert_{tc}$	μmol kg^{-1} m^{-1}	vertical ^{13}C gradient	calc. from dDIC/dz $\vert_{tc}$ and $d\delta^{13}$C/dDIC $\vert_{tc}$
K_z	m^2 s^{-1}	vertical diffusion coefficient at the base of the mixed layer	estimated from the vertical density gradient
DIC_{tc}	μmol kg^{-1}	DIC in thermocline box	calc. from l_{ent} and dDIC/dz $\vert_{tc}$
$^{13}r_{oc}$		^{13}C/^{12}C ratio of DIC	calc. from obs. $\delta^{13}C^{oc}$
$^{13}r_{atm}$		^{13}C/^{12}C ratio of atm. CO_2	calc. from obs. $\delta^{13}C^{atm}$
α_{eq}		equilibrium isotopic fract. of gas. CO_2 with respect to DIC	calc. from T
$DI^{13}C_{tc}$	μmol kg^{-1}	DI^{13}C in thermocline box	calc. from l_{ent}, dDIC/dz $\vert_{tc}$ and $d\delta^{13}$C/dDIC $\vert_{tc}$
dDI^{13}C/dx	μmol kg^{-1} m^{-1}	horizontal DI^{13}C gradient	calc. from dsDIC/dx and $d\delta^{13}$C/dx
$^{13}r_{org}$		^{13}C/^{12}C ratio of organic matter	calc. from fCO_2^{oc}, T and S

[a][1] [*Lukas and Karl*, 1999]; [2] NOAA-CIRES Climate Diagnostics Center, Boulder, Colorado (http://www.cdc.noaa.gov). For further details, see *Gruber et al.* [1998].
[b]To conform to *U.N. Educational, Scientific, and Cultural Organization* [1981], no unit is shown.
[c]The model computes the air-sea exchange of CO_2 on the basis of the air-sea difference of the CO_2 fugacities.

where $^{13}r_{grad}$ is the ^{13}C/^{12}C ratio of the horizontal gradients ($(d$DI^{13}C/$dx)/(d$DIC/$dx)$), with x denoting horizontal distance in the direction of the mean horizontal flow).

[94] Using independent estimates for the air-sea gas exchange, diffusion and entrainment as well as the observed temporal evolution of DIC and $\delta^{13}C^{oc}$, we thus have a set of four equations (C1)–(C4) which allow us to calculate the four unknown source terms (horizontal transport: J_{htr} and $^{13}J_{htr}$; and NCP: J_{ncp} and $^{13}J_{ncp}$). This mode of solving the equations is analogous to the ''double deconvolution'' method introduced by *Keeling et al.* [1989]. The calculations performed here differ from those used by *Gruber et al.* [1998], who prescribed horizontal transport and then solved the model equations for dDIC/dt, J_{ncp}, and $^{13}J_{ncp}$). A potential instability exists in solving the equations adopted here. It arises when the ratio of the horizontal gradients in DI^{13}C and DI^{12}C, i.e., $(d$DI^{13}C/$dx)/(d$DIC/$dx)$, approaches the ^{13}C/^{12}C ratio of organic matter (see detailed analysis in section C4). In this case, the system of equations essentially collapses to three equations with four unknowns. However, no such instability arises for the parameters and input values adopted in our study here.

C2. Input Variables and Parameters

[95] In addition to the observations described in the main text, we use physical and chemical data from a variety of sources as listed in Table C1. The diagnostic model is driven with smooth forcing functions created by fitting 3-harmonic curves in time with a least squares method to the linearly detrended time series of each input variable (see Table C2). Interannual variability in the forcing functions is accounted for by adding smoothing splines [*Enting*, 1987] that were fitted to the residuals of the harmonic fits. An overview of the input values and parameters used in the model is given in Tables C1 and C3. The uncertainty intervals adopted for the Monte Carlo runs are shown in Table C4. Unless mentioned otherwise, the methods and parameterizations used are those described by *Gruber et al.* [1998].

[96] Several additional input variables specifically needed for the application of the model to Station ALOHA were

Table C2. Harmonic Fitting Coefficients for Station ALOHA[a]

Parameter	Unit	H_0	a_1	b_1	a_2	b_2	a_3	b_3	R^2
sDIC	μmol kg^{-1}	1970.6	7.120	0.114	0.767	0.629	−0.017	0.943	0.78
sAlk	μmol kg^{-1}	2302.3	0.313	−0.240	−0.072	0.012	0.276	0.412	0.16
$\delta^{13}C^{oc}$	‰	1.396	−0.036	−0.009	−0.001	−0.004	−0.005	−0.007	0.90
$\delta^{13}C^{atm}$	‰	−7.965	−0.188	−0.001	0.057	−0.026	−0.001	0.004	0.89
$xCO_2^{atm\ b}$	ppm	361.88	3.62	−0.15	−0.95	0.69	0.04	−0.13	0.99
T	°C	24.82	−1.42	−0.59	−0.11	−0.08	0.08	−0.11	0.83
S		35.027	−0.026	0.050	−0.007	−0.023	−0.006	−0.001	0.27
h	m	60.29	−3.13	25.57	2.27	11.11	−1.34	3.66	0.68
ws	m s^{-1}	7.44	0.06	−0.59	−0.12	0.30	−0.43	−0.16	0.24
dDIC/$dz\vert_{tc}$	μmol kg^{-1} m^{-1}	0.645	−0.190	0.130	0.006	0.094	−0.052	−0.018	0.40
K_z	10^{-4} m^2 s^{-1}	0.175	0.110	0.021	0.024	−0.051	−0.011	0.006	0.38

[a]For a harmonic function of the form $H = \sum_{k=1}^{m}[a_k \sin\left(\frac{2\pi kt}{T}\right) + b_k \cos\left(\frac{2\pi kt}{T}\right)] + H_0$, where t is Julian day and T is the length of 1 year.
[b]Atmospheric mixing ratio in dry air.

Table C3. Definition and Standard Values of Parameters of the Diagnostic Box Model

Parameter	Value	Unit	Description	Source
ρ_0	1026.2	kg m^{-3}	average density of seawater	calculated from T and S
$^{13}r_s$	0.0112372		$^{13}C/^{12}C$ ratio of PDB standard	*Mook and Grootes* [1973]
α_{am}	0.99820		kinetic isotopic fractionation factor for the air-sea transfer of CO_2	*Keeling et al.* [1989]
$d\delta^{13}C/dDIC\|_{tc}$	−0.0063	‰ μmol^{-1} kg	ratio of vertical $\delta^{13}C$ and DIC gradient in the thermocline	calculated from CDRG obs.
l_{ent}	9	m	length scale of entrainment	based on h variability
dsDIC/dx	3.3×10^{-5}	μmol kg^{-1} m^{-1}	mean horizontal sDIC gradient	estimated from CDRG data
$d\delta^{13}C/dx$	-2.3×10^{-8}	‰ m^{-1}	mean horizontal $\delta^{13}C$ gradient	estimated from CDRG $\delta^{13}C$ data

established as follows. For the calculation of the exchange of CO_2 across the air-sea interface, we used atmospheric and oceanic fugacities of CO_2 rather than partial pressures, with the oceanic fCO_2 calculated from the same input data as oceanic pCO_2 using the routines of *DOE* [1994]. The relative humidity of air used to calculate fCO_2 in air was assumed to be 100% instead of the observed average humidity at the site (compare 89% for Bermuda [*DOE*, 1994, p. 687]) as a better approximation (R. Wanninkhof, personal communication, 2004).

[97] The calculation of the vertical fluxes by diffusion and entrainment requires knowledge of the vertical DIC and $\delta^{13}C^{oc}$ gradient below the mixed layer. The vertical DIC gradient was determined by a linear least squares fit to DIC data from the HOT program [*Lukas and Karl*, 1999] for each station over a 70-m interval below the mixed layer. This gradient varies between 0.4 μmol kg^{-1}m in spring and 0.8 μmol kg^{-1}m in winter (see Figure C1a). As we have sampled only one profile of $\delta^{13}C^{oc}$ at Station ALOHA, we estimated the vertical gradient of $\delta^{13}C^{oc}$ indirectly by first determining the vertical relationship between DIC and $\delta^{13}C^{oc}$ for this one profile and then multiplying the obtained ratio with the time varying vertical gradient of DIC. A linear least squares fit of $\delta^{13}C^{oc}$ versus DIC for our single profile data from the thermocline between 100 m and 500 m depth yields a slope of -0.0063 ± 0.0005‰ μmol^{-1} kg (see Figure C2). Data from nearby cruises of the World Ocean Circulation Experiment (WOCE) (data from R. M. Key, personal communication, 2003), also plotted in Figure C2, show a similar linear relation.

[98] The vertical diffusion coefficient, K_z, at the base of the mixed layer (Figure C1b) was estimated on the basis of the vertical density gradient just below the surface mixed layer [*Denman and Gargett*, 1983]. The high degree of variability in the data with K_z values up to 1.2×10^{-4} m^2 s^{-1} may be largely caused by short-term events like the passage of storms and eddies. For the summer and the early autumn season, when vertical stratification is strong, K_z shows consistently low values of about 0.1×10^{-4} m^2 s^{-1}. In winter the smoothed representation of the seasonal cycle gives values as high as 0.4×10^{-4} m^2 s^{-1}. Our values are, except for the winter, substantially smaller than the effective annual mean vertical diffusivity of 0.5×10^{-4} m^2 s^{-1} inferred by *Quay and Stutsman* [2003] on the basis of their diagnostic carbon cycle study. While measurements during an extreme event, i.e., the passage of a large storm in the North Pacific, have shown values of this magnitude and even larger [*Large et al.*, 1986], most microstructure measurements [*Denman and Gargett*, 1983; *Gregg*, 1987; *Toole et al.*, 1994; *Polzin et al.*, 1995] and oceanic tracer release experiments [*Ledwell et al.*, 1993, 1998] suggest that vertical diffusivities in the thermocline of the midlatitudes are small, of the order of 0.1×10^{-4} m^2 s^{-1}.

[99] The computation of horizontal transport processes requires an estimate of the horizontal sDIC and $\delta^{13}C^{oc}$ gradients in the direction of the mean horizontal flow. The mean meridional sDIC gradient was determined by us from surface sDIC data from WOCE cruises P15N and P16N (http://whpo.ucsd.edu) between 20°N and 28°N. A linear least squares fit of sDIC to latitude gives $(3.3 \pm 0.6) \times 10^{-5}$ μmol kg^{-1} m^{-1}. A second method to determine the horizontal sDIC gradient on the basis of a surface sDIC climatology computed from SST and surface salinity [following *Lee et al.*, 2000b] yields a similar value. The horizontal gradient of $\delta^{13}C^{oc}$ was determined from $\delta^{13}C^{oc}$ measurements by CDRG taken during seven cruises (NOAA85, PRPS82, PRPS85, GC92, FGGE, ROUN, and TUNE [*Gruber et al.*, 1999]) that sampled the region around Hawaii between 1979 and 1992. All data were adjusted to 1995 using a ^{13}C Suess effect of

Table C4. Initial Values and Uncertainties of Parameters Used for the Monte Carlo Simulations

Parameter	Standard Value	Standard Deviation	Unit	Description
$d\delta^{13}C/dDIC\|_{tc}$	−0.0063	0.0005	‰ μmol^{-1} kg	ratio of vertical $\delta^{13}C$ and DIC gradient
l_{ent}	9	3	m	length scale of entrainment
dsDIC/dx	3.3×10^{-5}	0.6×10^{-5}	μmol kg^{-1} m^{-1}	mean horizontal sDIC gradient
$d\delta^{13}C/dx$	-2.3×10^{-8}	3.5×10^{-8}	‰ m^{-1}	mean horizontal $\delta^{13}C$ gradient
β_{ex}	1.0	0.1		multiplication factor for gas exchange
β_{diff}	1.0	0.5		multiplication factor for vert. diffusion
ΔfCO_2^{oc}	0.0	1.0	μatm	correction term for fCO_2^{oc}
$\Delta dDIC/dz\|_{tc}$	0.0	0.1	μmol kg^{-1} m^{-1}	correction term for $dDIC/dz\|_{tc}$
$\Delta^{13}r_{org}$	0.0	0.00003		correction term for $^{13}r_{org}$

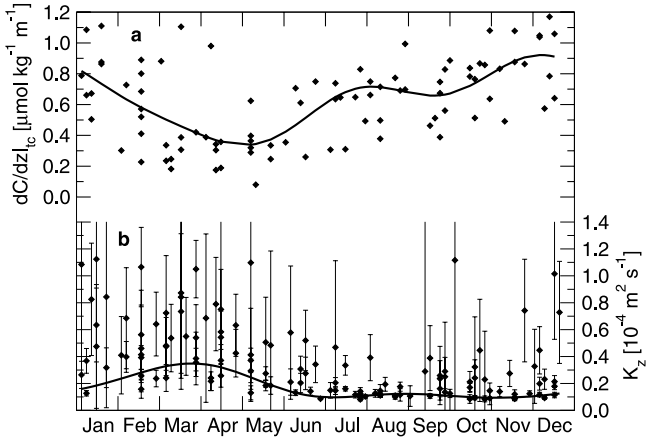

Figure C1. Seasonal composite time series. (a) Vertical DIC gradient at the base of the mixed layer. The diamonds denote the observations and the line shows the results of a 3-harmonic fit. (b) Time series for the vertical diffusion coefficient K_z at the base of the mixed layer. The diamonds show the average K_z for all casts of a particular cruise; the error bars give the standard deviations. The line denotes a 3-harmonic fit.

-0.020‰ yr^{-1} [*Bacastow*, 1996; *Gruber et al.*, 1999]. A latitudinal gradient of $(-2.3 \pm 3.5) \times 10^{-8}$ ‰ m^{-1} was determined from the adjusted values between 18°N and 29°N. The east-west gradients of DIC and $\delta^{13}C^{oc}$ were found to be small and were neglected.

C3. Numerical Implementation

[100] The diagnostic model equations (C1)–(C4) are solved for small time steps (400 per year) from July 1988 until June 2002. To address uncertainties in the model parameters, Monte Carlo experiments [*Rubinstein*, 1981] were performed (see *Gruber et al.* [1998] for details), in which a random set of values were chosen from the parameter set shown in Table C4 for each simulation. From the results of these runs, a standard deviation was computed for each term and for each time step of the model. For the results reported here, the average seasonal cycle and fluxes was extracted from these simulations.

C4. Numerical Instability

[101] The diagnostic box-model can be successfully implemented, provided that net community production (NCP) and horizontal transport have different isotopic signatures, i.e., that the $^{13}C/^{12}C$ of their source terms differs so that the model consists of a system of four equations (C1)–(C4) and four unknowns. However, if isotopic ratio of organic matter $^{13}r_{org}$ (see equation (C3)) and the isotopic ratio of the horizontal gradient $^{13}r_{grad}$ (see equation (C4)) are numerically equal or nearly the same, the system has an undetermined solution. We describe here how this instability arises. Note that this problem exists only when the diagnostic model is solved as described in this study; it does not arise when horizontal transport is prescribed as in the study of *Gruber et al.* [1998].

[102] We start with the four main equations of the model as given in the main text (see equations (C1)–(C4)). Summing the first three terms of equation (C1) to

$$J_p = J_{ex} + J_{diff} + J_{ent}, \tag{C5}$$

and the first three terms of equation (C2) to

$$^{13}J_p = {}^{13}J_{ex} + {}^{13}J_{diff} + {}^{13}J_{ent}, \tag{C6}$$

and using our parameterization for J_{htr} and $^{13}J_{htr}$, we get

$$\frac{d\mathrm{DIC}}{dt} = J_p + u\frac{d\mathrm{DIC}}{dx} + J_{ncp} \tag{C7}$$

$$\frac{d\mathrm{DI}^{13}\mathrm{C}}{dt} = {}^{13}J_p + u\frac{d\mathrm{DI}^{13}\mathrm{C}}{dx} + {}^{13}J_{ncp}, \tag{C8}$$

where u is the horizontal velocity, and dDIC/dx and $d\mathrm{DI}^{13}\mathrm{C}/dx$ denote the horizontal gradients of DIC and $\mathrm{DI}^{13}\mathrm{C}$, respectively. We thus reduce the system to three equations (C3), (C7), and (C8) and three unknowns

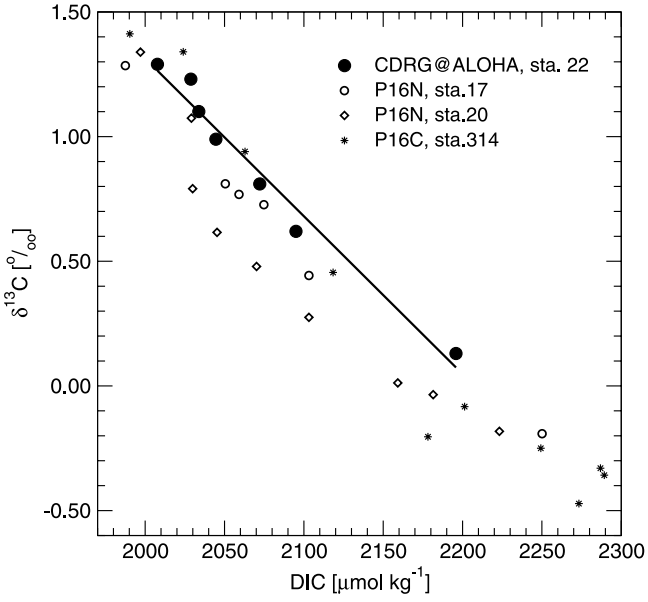

Figure C2. DIC versus $\delta^{13}C^{oc}$ values for the thermocline between 100 m and 500 m depth at Station ALOHA. The solid circles represent measurements taken on 17 December 1990 during HOT cruise 22. The line shows a linear regression of these values yielding a slope of -0.0063 ± 0.0005‰ μmol^{-1} kg. For comparison, data from nearby World Ocean Circulation Experiment (WOCE) cruises (R. M. Key, personal communication, 2003) are shown: P16N, station 17 (8 March 1991 at 20°23′N, 154°14′W, circles), P16N, station 20 (10 March 1991 at 21°55′N, 15°20′W, diamonds), and P16C, station 314 (28 September 1991 at 16°48′N, 153°16′W, stars).

(J_{ncp},$^{13}J_{ncp}$, u) Our goal is to solve for J_{ncp}. Equation (C7) can be rearranged for J_{ncp},

$$J_{ncp} = \frac{d\mathrm{DIC}}{dt} - u\frac{d\mathrm{DIC}}{dx} - J_p. \tag{C9}$$

Solving equation (C8) for u gives

$$u = \frac{\frac{d\mathrm{DI}^{13}\mathrm{C}}{dt} - {}^{13}J_p - {}^{13}J_{ncp}}{\frac{d\mathrm{DI}^{13}\mathrm{C}}{dx}}. \tag{C10}$$

[103] Inserting equations (C10) and (C3) into equation (C9) yields

$$J_{ncp} = \frac{d\mathrm{DIC}}{dt} - \frac{\frac{d\mathrm{DI}^{13}\mathrm{C}}{dt} - {}^{13}J_p - \frac{{}^{13}r_{org}}{1+{}^{13}r_{org}}J_{ncp}}{\frac{d\mathrm{DI}^{13}\mathrm{C}}{dx}}\frac{d\mathrm{DIC}}{dx} - J_p. \tag{C11}$$

Solving for J_{ncp} gives

$$J_{ncp} = \frac{\frac{d\mathrm{DI}^{13}\mathrm{C}}{dx}\left[\frac{d\mathrm{DIC}}{dt} - J_p\right] - \frac{d\mathrm{DIC}}{dx}\left[\frac{d\mathrm{DI}^{13}\mathrm{C}}{dt} - {}^{13}J_p\right]}{\frac{d\mathrm{DI}^{13}\mathrm{C}}{dx} - \frac{{}^{13}r_{org}}{1+{}^{13}r_{org}}\frac{d\mathrm{DIC}}{dx}}. \tag{C12}$$

[104] This is the final form of the equation as solved by the diagnostic model for each step. The solution for the source term for net community production J_{ncp} is undetermined when denominator is equal to 0, which is the case for

$$\frac{d\mathrm{DI}^{13}\mathrm{C}}{dx} = \frac{{}^{13}r_{org}}{1+{}^{13}r_{org}}\frac{d\mathrm{DIC}}{dx}, \tag{C13}$$

i.e., for

$$\frac{{}^{13}r_{org}}{1+{}^{13}r_{org}} = \frac{\frac{d\mathrm{DI}^{13}\mathrm{C}}{dx}}{\frac{d\mathrm{DIC}}{dx}} = \frac{{}^{13}r_{grad}}{1+{}^{13}r_{grad}}, \tag{C14}$$

which is the case for

$${}^{13}r_{org} = {}^{13}r_{grad}. \tag{C15}$$

[105] Equation (C15) indicates that the solution of the diagnostic model, as used here, is undetermined when the $^{13}C/^{12}C$ isotopic value of organic matter is equal to the isotopic signature of the horizontal gradients. In the case of Station ALOHA, the isotopic values are well separated, and this potential caveat does not pose a problem.

[106] **Acknowledgments.** We are indebted to the members of the Carbon Dioxide Research Group at the Scripps Institution of Oceanography who were responsible for sampling, measurement, and management of the carbon data used in this study, in particular, Peter Guenther, Guy Emanuele, David Moss, and Alane Bollenbacher. Also, at the Scripps Institution, we thank Andrew Dickson and Tim Lueker for technical advice on the chemistry of seawater, and members of the Oceanographic Data Facility for the shore analysis of additional properties of seawater. We are very grateful to Dave Karl, Chris Winn, John Dore, Chris Sabine, and many others for their help in collecting water samples at Station ALOHA and supporting our efforts. Discussions with John Dore, Yi Chao, Hartmut Frenzel, Kasper Plattner, and Anita Leinweber have helped to sharpen the ideas presented here. We thank Paul Quay and an anonymous reviewer for their constructive and supportive comments. N. G. and H. B. acknowledge support from the U.S. National Science Foundation (OCE-0097337); C. D. K. acknowledges support from OCE-0083918 and ATM-0120527.

References

Abell, J., S. Emerson, and P. Renaud (2000), Distributions of TOP, TON, and TOC in the North Pacific subtropical gyre: Implications for nutrient supply in the surface ocean and remineralization in the upper thermocline, *J. Mar. Res.*, *58*(2), 203–222.

Bacastow, R. B. (1996), The effect of temperature change of warm surface waters of the oceans on atmospheric CO_2, *Global Biogeochem. Cycles*, *10*(2), 319–333.

Bacastow, R., and C. Keeling (1979), Models to predict future atmospheric CO_2 concentrations, in *Workshop on the Global Effects of Carbon Dioxide from Fossil Fuels*, edited by W. P. Elliott and L. Machta, pp. 72–90, U.S. Dep. of Energy, Washington, D. C.

Bacastow, R. B., C. D. Keeling, T. J. Lueker, M. Wahlen, and W. G. Mook (1996), The ^{13}C Suess effect in the world surface oceans and its implications for oceanic uptake of CO_2: Analysis of observations at Bermuda, *Global Biogeochem. Cycles*, *10*(2), 335–346.

Bates, N. R. (2001), Interannual variability of oceanic CO_2 and biogeochemical properties in the western North Atlantic Subtropical gyre, *Deep Sea Res., Part II*, *48*, 1507–1528.

Bates, N. R., A. F. Michaels, and A. H. Knap (1996), Seasonal and interannual variability of oceanic carbon dioxide species at the U.S. JGOFS Bermuda Atlantic Time-series Study (BATS) site, *Deep Sea Res.*, *Part II*, *43*, 347–383.

Bates, N. R., A. C. Pequignet, R. J. Johnson, and N. Gruber (2002), A variable sink for atmospheric CO_2 in Subtropical Mode Water of the North Atlantic Ocean, *Nature*, *420*, 489–493.

Benitez-Nelson, C., K. Buesseler, D. Karl, and J. Andrews (2001), A time-series study of particulate matter export in the North Pacific Subtropical Gyre based on ^{234}Th:^{238}U disequilibrium, *Deep Sea Res.*, *Part I*, *48*, 2595–2611.

Bollenbacher, A. F., C. D. Keeling, E. F. Stewart, M. Wahlen, and T. P. Whorf (1998), Calibration methodology for the Scripps $^{13}C/^{12}C$ and $^{18}O/^{16}O$ stable isotope program, technical report, Scripps Inst. of Oceanogr., La Jolla, Calif.

Bond, N. A., J. E. Overland, M. Spillane, and P. Stabeno (2003), Recent shifts in the state of the North Pacific, *Geophys. Res. Lett.*, *30*(23), 2183, doi:10.1029/2003GL018597.

Brix, H., N. Gruber, and C. D. Keeling (2004), Interannual variability of the upper ocean carbon cycle at station ALOHA near Hawaii, *Global Biogeochem. Cycles*, doi:10.1029/2004GB002245, in press.

Broecker, W. S., and T.-H. Peng (1974), Gas exchange rates between air and sea, *Tellus*, *26*, 21–35.

Chao, Y., M. Ghil, and J. C. McWilliams (2000), Pacific interdecadal variability in this century's sea surface temperature, *Geophys. Res. Lett.*, *27*(15), 2261–2264.

Chavez, F. P., J. Ryan, S. E. Lluch-Cota, and M. Ñiquen C. (2003), From anchovies to sardines and back: Multidecadal change in the Pacific Ocean, *Science*, *299*, 217–221.

Craig, H. (1957), Isotopic standards for carbon and oxgyen and correction factors for mass-spectrometric analysis of carbon dioxide, *Geochim. Cosmochim. Acta*, *12*, 133–149.

Denman, K. L., and A. E. Gargett (1983), Time and space scales of vertical mixing and advection of phytoplankton in the upper ocean, *Limnol. Oceanogr.*, *28*(5), 801–815.

Denman, K. L., and A. E. Gargett (1995), Biological-physical interactions in the upper ocean: The role of vertical and small scale transport processes, *Annu. Rev. Fluid Mech.*, *27*, 225–255.

Deutsch, C. D., N. Gruber, R. M. Key, A. Ganachaud, and J. L. Sarmiento (2001), Denitrification and N_2 fixation in the Pacific Ocean, *Global Biogeochem. Cycles*, *15*(2), 483–506.

Dore, J., P. R. Guenther, C. D. Keeling, and D. Karl (2001), DIC, TAlk, the clock strikes twelve: HOT-SIO intercomparison completes first dozen years, *U.S. JGOFS News*, *11*(2), 3–8.

Dore, J. E., R. Lukas, D. W. Sadler, and D. M. Karl (2003), Climate-driven changes to the atmospheric CO_2 sink in the subtropical North Pacific Ocean, *Nature*, *424*, 754–757.

Duce, R. A., et al. (1991), The atmospheric input of trace species to the world ocean, *Global Biogeochem. Cycles*, *5*(3), 193–259.

Emerson, S., P. Quay, D. Karl, C. Winn, and L. Tupas (1997), Experimental determination of the organic carbon flux from open-ocean surface waters, *Nature*, *389*, 951–954.

Emerson, S., S. Mecking, and J. Abell (2001), The biological pump in the subtropical North Pacific ocean: Nutrient sources, Redfield ratios and recent changes, *Global Biogeochem. Cycles*, *15*(3), 535–554.

Enting, I. G. (1987), On the use of smoothing splines to filter CO_2 data, *J. Geophys. Res.*, *92*(D9), 10,977–10,984.

Esbensen, S. K., and J. Kushnir (1981), The heat budget of the global oceans: An atlas based on estimates from marine surface observations, *Rep. 29*, Clim. Res. Inst., Oregon State Univ., Corvallis.

Feely, R. A., R. Wanninkhof, T. Takahashi, and P. Tans (1999), Influence of El Niño on the equatorial Pacific contribution to atmospheric CO_2 accumulation, *Nature*, *398*, 597–601.

Follows, M. J., R. G. Williams, and J. C. Marshall (1996), The solubility pump of carbon in the subtropical gyre of the north Atlantic, *J. Mar. Res.*, *54*, 605–630.

Gloor, M., N. Gruber, J. L. Sarmiento, C. L. Sabine, R. A. Feely, and C. Roedenbeck (2003), A first estimate of present and pre-industrial air-sea CO_2 fluxes patterns based on ocean interior carbon measurements and models, *Geophys. Res. Lett.*, *30*(1), 1010, doi:10.1029/2002GL015594.

Gregg, M. C. (1987), Diapycnal mixing in the thermocline: A review, *J. Geophys. Res.*, *92*(C5), 5249–5286.

Gruber, N., and C. D. Keeling (2001), An improved estimate of the isotopic air-sea disequilibrium of CO_2: Implications for the oceanic uptake of anthropogenic CO_2, *Geophys. Res. Lett.*, *28*(3), 555–558.

Gruber, N., and J. L. Sarmiento (2002), Biogeochemical/physical interactions in elemental cycles, in *THE SEA*, vol. 12, *Biological-Physical Interactions in the Oceans*, edited by A. R. Robinson, J. J. McCarthy, and B. J. Rothschild, pp. 337–399, John Wiley, Hoboken, N. J.

Gruber, N., C. D. Keeling, and T. F. Stocker (1998), Carbon-13 constraints on the seasonal inorganic carbon budget at the BATS site in the northwestern Sargasso Sea, *Deep Sea Res.*, *Part I*, *45*, 673–717.

Gruber, N., C. D. Keeling, R. B. Bacastow, P. R. Guenther, T. J. Lueker, M. Wahlen, H. A. J. Meijer, W. G. Mook, and T. F. Stocker (1999), Spatiotemporal patterns of carbon-13 in the global surface oceans and the oceanic Suess effect, *Global Biogeochem. Cycles*, *13*(2), 307–335.

Gruber, N., N. Bates, and C. D. Keeling (2002), Interannual variability in the North Atlantic carbon sink, *Science*, *298*, 2374–2378.

Gurney, K. R., et al. (2002), Towards robust regional estimates of CO_2 sources and sinks using atmospheric transport models, *Nature*, *415*, 626–630.

Heimann, M. (1995), Dynamics of the carbon cycle, *Nature*, *375*, 629–630.

Johnson, G. C. (2001), The Pacific Ocean subtropical cell surface limb, *Geophys. Res. Lett.*, *28*(9), 1771–1774.

Kalnay, E., et al. (1996), The NCEP/NCAR 40-year reanalysis project, *Bull. Am. Meteorol. Soc.*, *77*(3), 437–471.

Karl, D. M. (1999), A sea of change: Biogeochemical variability in the North Pacific subtropical gyre, *Ecosystems*, *2*(3), 181–214.

Karl, D. M., and R. Lukas (1996), The Hawaii Ocean Time-series (HOT) program: Background, rationale and field implementation, *Deep Sea Res.*, *Part II*, *43*, 129–156.

Karl, D. M., R. Letelier, D. Hebel, L. Tupas, J. Dore, J. Christian, and C. Winn (1995), Ecosystem changes in the North Pacific subtropical gyre attributed to the 1991–92 El Niño, *Nature*, *373*, 230–234.

Karl, D. M., J. R. Christian, J. E. Dore, D. V. Hebel, R. M. Letelier, L. M. Tupas, and C. D. Winn (1996), Seasonal and interannual variability in primary production and particle flux at station ALOHA, *Deep Sea Res.*, *Part II*, *43*, 539–568.

Karl, D., R. Letelier, L. Tupas, J. Dore, J. Christian, and D. Hebel (1997), The role of nitrogen fixation in the biogeochemical cycling in the subtropical North Pacific Ocean, *Nature*, *388*, 533–538.

Karl, D. M., R. R. Bidigare, and R. M. Letelier (2001), Long-term changes in plankton community structure and productivity in the North Pacific Subtropical Gyre: The domain shift hypothesis, *Deep Sea Res.*, *Part II*, *48*, 1449–1470.

Karl, D. M., et al. (2002), Dinitrogen fixation in the world's ocean, *Biogeochemistry*, *57/58*, 47–98.

Keeling, C. D. (1979), The Suess Effect: ^{13}Carbon and ^{14}Carbon interactions, in *Environment International*, vol. 2, pp. 229–300, Pergamon, New York.

Keeling, C. D. (1993), NATO lecture 2: Surface ocean CO_2, in *The Global Carbon Cycle*, edited by M. Heimann, pp. 413–430, Springer-Verlag, New York.

Keeling, C. D., R. B. Bacastow, A. F. Carter, S. C. Piper, T. P. Whorf, M. Heimann, W. G. Mook, and H. Roeloffzen (1989), A three-dimensional model of atmospheric CO_2 transport based on observed winds: 1. Analysis of observational data, in *Aspects of Climate Variability in the Pacific and the Western Americas*, *Geophys. Monogr. Ser.*, vol. 55, edited by D. H. Peterson, pp. 165–237, AGU, Washington, D. C.

Large, W. G., J. C. McWilliams, and P. P. Niiler (1986), Upper ocean thermal response to strong autumnal forcing of the Northeast Pacific, *J. Phys. Oceanogr.*, *16*, 1524–1550.

Large, W. G., J. C. McWilliams, and S. C. Doney (1994), Oceanic vertical mixing: A review and a model with a nonlocal boundary layer parameterization, *Rev. Geophys.*, *32*, 363–403.

Ledwell, J. R., A. J. Watson, and C. S. Law (1993), Evidence for slow mixing across the pycnocline from an open-ocean tracer-release experiment, *Nature*, *364*, 701–703.

Ledwell, J., A. Watson, and C. Law (1998), Mixing of a tracer in the pycnocline, *J. Geophys. Res.*, *103*(C10), 21,499–21,529.

Lee, K., R. J. Millero, R. H. Byrne, R. A. Feely, and R. Wanninkhof (2000a), The recommended dissociation constants for carbonic acid in seawater, *Geophys. Res. Lett.*, *27*(2), 229–232.

Lee, K., R. Wanninkhof, R. A. Feely, F. J. Millero, and T.-H. Peng (2000b), Global relationships of total inorganic carbon with temperature and nitrate in surface seawater, *Global Biogeochem. Cycles*, *14*(3), 979–994.

Letelier, R. M., D. M. Karl, M. R. Abbott, P. Flament, M. Freilich, R. Lukas, and T. Strub (2000), Role of late winter mesoscale events in the biogeochemical variability of the upper water column of the North Pacific Subtropical Gyre, *J. Geophys. Res.*, *105*(C12), 28,723–28,739.

Lomas, M., N. Bates, A. Knap, D. Karl, R. Lukas, M. Landry, R. Bidigare, D. Steinberg, and C. Carlson (2002), Refining our understanding of oceanic biogeochemistry and ecosystem functioning, *Eos Trans. AGU*, *83*(48), 559–567.

Lueker, T. J. (1998), The ratio of the first and second dissociation constants of carbonic acid determined from the concentration of carbon dioxide in gas and seawater at equilibrium, Ph.D. thesis, Scripps Inst. of Oceanogr., Univ. of Calif., San Diego.

Lueker, T., A. Dickson, and C. Keeling (2000), Ocean pCO_2 calculated from dissolved inorganic carbon, alkalinity, and equations for K_1 and K_2: Validation based on laboratory measurements of CO_2 in gas and seawater at equilibrium, *Mar. Chem.*, *70*, 105–119.

Lukas, R., and D. Karl (1999), Hawaii Ocean Time-series (HOT), 1988–1998: A decade of interdisciplinary oceanography [CD-ROM], *Tech. Rep. 99-05*, School of Ocean and Earth Sci. and Technol., Univ. of Hawaii. (Updates available at http://hahana.soest.hawaii.edu/hot/hot.html)

Lynch-Stieglitz, J., T. F. Stocker, W. S. Broecker, and R. G. Fairbanks (1995), The influence of air-sea exchange on the isotopic composition of oceanic carbon: Observations and modeling, *Global Biogeochem. Cycles*, *9*(4), 653–665.

Mantua, N., and S. Hare (2002), The Pacific Decadal Oscillation, *J. Oceanogr.*, *58*(1), 35–44.

Mantua, N., S. Hare, Y. Zhang, J. Wallace, and R. Francis (1997), A Pacific interdecadal climate oscillation with impacts on salmon production, *Bull. Am. Meteorol. Soc.*, *78*(6), 1069–1079.

Mehrbach, C., C. H. Culberson, J. E. Hawley, and R. M. Pytkowicz (1973), Measurement of the apparent dissociation constants of carbonic acid in seawater at atmospheric pressure, *Limnol. Oceanogr.*, *18*, 897–907.

Michaels, A. F., and A. H. Knap (1996), Overview of the U.S. JGOFS Bermuda Atlantic Time-series Study and the Hydrostation S program, *Deep Sea Res.*, *Part II*, *43*, 157–198.

Millero, F. J., K. Lee, and M. P. Roche (1998), The distribution of total alkalinity in the surface waters, *Mar. Chem.*, *60*, 111–130.

Mook, W. G., and P. M. Grootes (1973), The measuring procedure and corrections for the high-precision mass-spectrometric analysis of isotopic abundance ratios, especially referring to carbon, oxygen and nitrogen, *Int. J. Mass Spectrom. Phys.*, *12*, 273–298.

Neuer, S., R. Davenport, T. Freudenthal, G. Wefer, O. Llinás, M.-J. Rueda, D. K. Steinberg, and D. M. Karl (2002), Differences in the biological carbon pump at three subtropical ocean sites, *Geophys. Res. Lett.*, *29*(18), 1885, doi:10.1029/2002GL015393.

Polzin, K., J. M. Toole, and R. W. Schmitt (1995), Finescale parameterizations of turbulent dissipation, *J. Phys. Oceanogr.*, *25*(3), 306–328.

Prentice, I. C., et al. (2001), The carbon cycle and atmospheric CO_2, in *IPCC WGI Third Assessment Report*, pp. 183–237, Cambridge Univ. Press, New York.

Quay, P., and J. Stutsman (2003), Surface layer carbon budget for the subtropical N. Pacific: $\delta^{13}C$ constraints at Station ALOHA, *Deep Sea Res., Part I*, *50*, 1045–1061.

Roeloffzen, J. C. (1993), The calibration of ^{13}C and ^{18}O measurements, 1977–1991, internal report, Cent. for Isotope Phys., Groningen, Netherlands.

Rubinstein, R. Y. (1981), *Simulation and the Monte Carlo method*, John Wiley, Hoboken, N. J.

Sabine, C. L., F. T. Mackenzie, C. Winn, and D. M. Karl (1995), Geochemistry of carbon dioxide in seawater at the Hawaii ocean time series station, ALOHA, *Global Biogeochem. Cycles*, *9*(4), 637–651.

Sabine, C. L., D. W. R. Wallace, and F. J. Millero (1997), Survey of CO_2 in the oceans reveals clues about global carbon cycle, *Eos Trans. AGU*, *78*(5), 49–55.

Sarmiento, J. L., and N. Gruber (2004), *Ocean Biogeochemical Dynamics*, Princeton Univ. Press, Princeton, N. J., in press.

Sonnerup, R., P. D. Quay, and J. Bullister (1999), North Pacific thermocline ventilation rates estimated from CFC and bomb-radiocarbon WOCE results, *Deep Sea Res.*, *Part I*, *46*, 777–805.

Sonnerup, R. E., P. D. Quay, A. P. McNichol, J. L. Bullister, T. A. Westby, and H. L. Anderson (2000), The Indian Ocean Suess effect, *Global Biogeochem. Cycles*, *14*(3), 903–916.

Sprintall, J., and M. Tomczak (1992), Evidence of barrier layer in the surface layer of the tropics, *J. Geophys. Res.*, *97*(C5), 7305–7316.

Stammer, D., C. Wunsch, R. Giering, C. Eckert, P. Heimbach, J. Marotzke, A. Adcroft, C. Hill, and J. Marshall (2002), The global ocean circulation during 1992–1997, estimated from ocean observations and a general circulation model, *J. Geophys. Res.*, *107*(C9), 3118, doi:10.1029/2001JC000888.

Takahashi, T., W. Broecker, S. Werner, and A. E. Bainbridge (1980), Carbonate chemistry of the surface waters of the world oceans, in *Isotope Marine Chemistry*, edited by E. D. Goldberg, Y. Horibe, and K. Saruhashi, pp. 291–326, Uchida Rokakuho, Tokyo.

Takahashi, T., J. Olafsson, J. G. Goddard, D. W. Chipman, and S. C. Sutherland (1993), Seasonal variation of CO_2 and nutrients in the high-latitude surface oceans: A comparative study, *Global Biogeochem. Cycles*, *7*(4), 843–878.

Takahashi, T., et al. (2002), Global sea-air CO_2 flux based on climatological surface ocean pCO_2, and seasonal biological and temperature effects, *Deep Sea Res.*, *Part II*, *49*, 1601–1622.

Takahashi, T., S. C. Sutherland, R. A. Feely, and C. E. Cosca (2003), Decadal variation of the surface water pCO_2 in the western and eastern equatorial Pacific, *Science*, *302*, 852–856.

Tomczak, M., and J. S. Godfrey (2003), *Regional Oceanography: An Introduction*, 2nd ed., 390 pp., Daya, Delhi, India.

Toole, J. M., K. L. Polzin, and R. W. Schmitt (1994), Estimates of diapycnal mixing in the abyssal ocean, *Science*, *264*, 1120–1123.

Trenberth, K. (1990), Recent observed interdecadal climate changes in the Northern Hemisphere, *Bull. Am. Meteorol. Soc.*, *71*, 988–993.

U.N. Educational, Scientific, and Cultural Organization (1981), Background papers and supporting data on the practical salinity scale, *Tech. Pap. Mar. Sci.*, *37*, Paris.

U.S. Department of Energy (1994), Handbook of methods for the analysis of the various parameters of the carbon dioxide system in sea water; version 2, *Tech. Rep. ORNL/CDIAC-74*, Carbon Dioxide Inf. Anal. Cent., Oak Ridge Natl. Lab., Oak Ridge, Tenn.

Villareal, T. A., C. Pilskaln, M. Brzezinski, F. Lipschultz, M. Dennett, and G. B. Gardner (1999), Upward transport of oceanic nitrate by migrating diatom mats, *Nature*, *397*, 423–425.

Wallace, D. W. R. (2001), Storage and transport of excess CO_2 in the oceans: The JGOFS/WOCE global CO_2 survey, in *Ocean Circulation and Climate*, edited by G. Siedler, J. Church, and J. Gould, pp. 489–524, Academic, San Diego, Calif.

Wanninkhof, R., S. Doney, T. Takahashi, and W. McGillis (2001), The effect of using time-averaged winds on regional air-sea CO_2 fluxes, in *Gas Transfer at Water Surfaces*, *Geophys. Monogr. Ser.*, vol. 127, edited by M. Donelan et al., pp. 351–357, AGU, Washington, D. C.

Williams, P. J. L. (1993), On the definition of plankton production terms, *ICES Mar. Sci. Symp.*, *197*, 9–19.

Winn, C. D., F. T. Mackenzie, C. J. Carrillo, C. L. Sabine, and D. M. Karl (1994), Air-sea carbon dioxide exchange in the North Pacific subtropical gyre: Implications for the global carbon budget, *Global Biogeochem. Cycles*, *8*(2), 157–163.

Winn, C., Y.-H. Li, F. T. Mackenzie, and D. M. Karl (1998), Rising surface ocean dissolved inorganic carbon at the Hawaii Ocean Time-series site, *Mar. Chem.*, *60*, 33–47.

H. Brix and N. Gruber (corresponding author), Department of Atmospheric and Oceanic Sciences and IGPP, 5853 Slichter Hall, University of California, Los Angeles, Los Angeles, CA 90095-1567, USA. (hbrix@igpp.ucla.edu; ngruber@igpp.ucla.edu)

C. D. Keeling, Scripps Institution of Oceanography, University of California, San Diego, La Jolla, CA 92093-0220, USA. (cdkeeling@ucsd.edu)

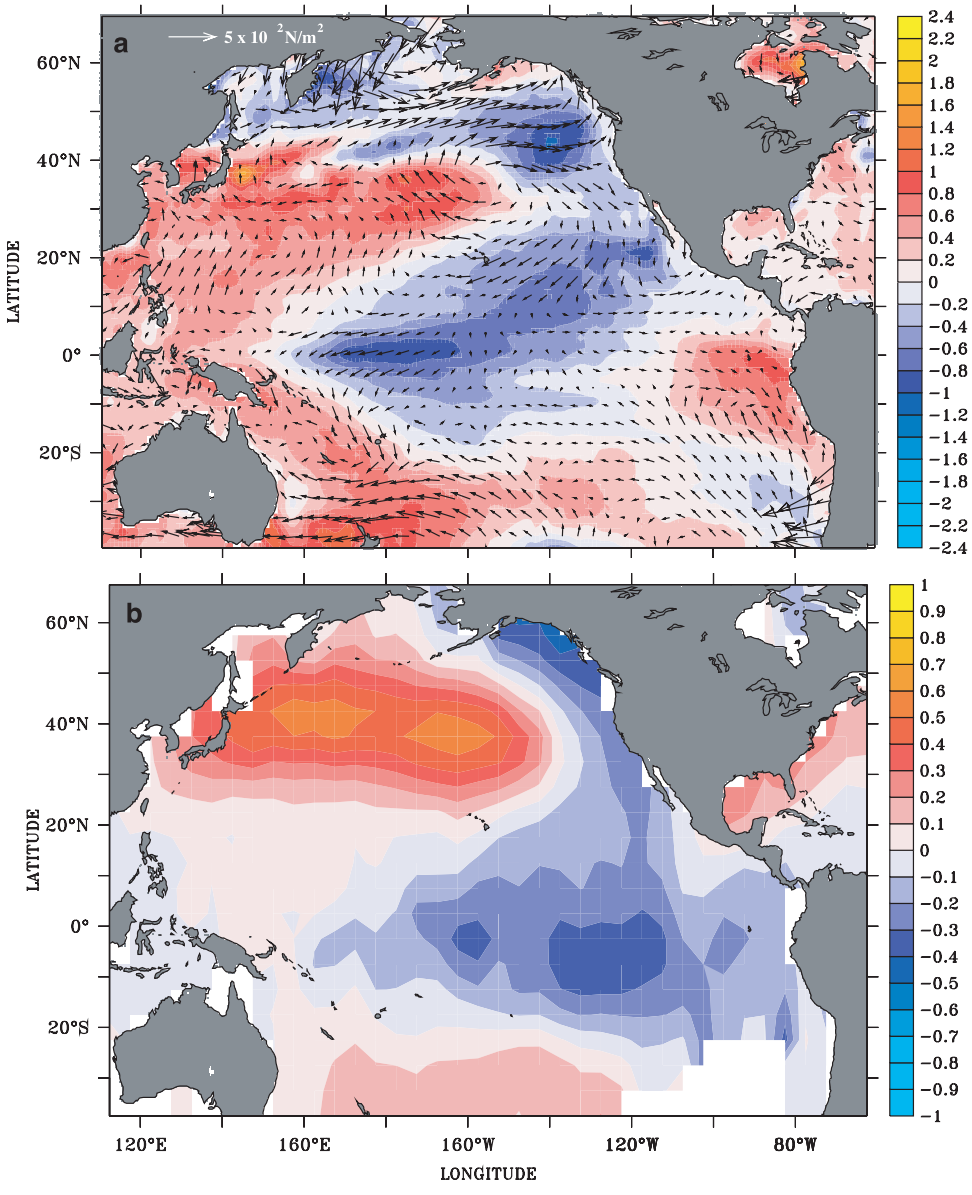

Figure 3. Pattern of climate change in the North Pacific. (a) Difference between 5-year mean SST (monthly mean Reynolds OI data in °C, shaded) and wind stress anomalies (monthly mean NCEP Reanalysis data in N/m^2, arrows) for 1997–2001 minus 1992–1996. (b) Map of the regression coefficient of SST anomalies versus a dimensionless PDO index [*Mantua et al.*, 1997]. The regression coefficient has been inverted in order to emphasize the similarity to Figure 3a. Units are °C per unit standard deviation. See text for data sources.

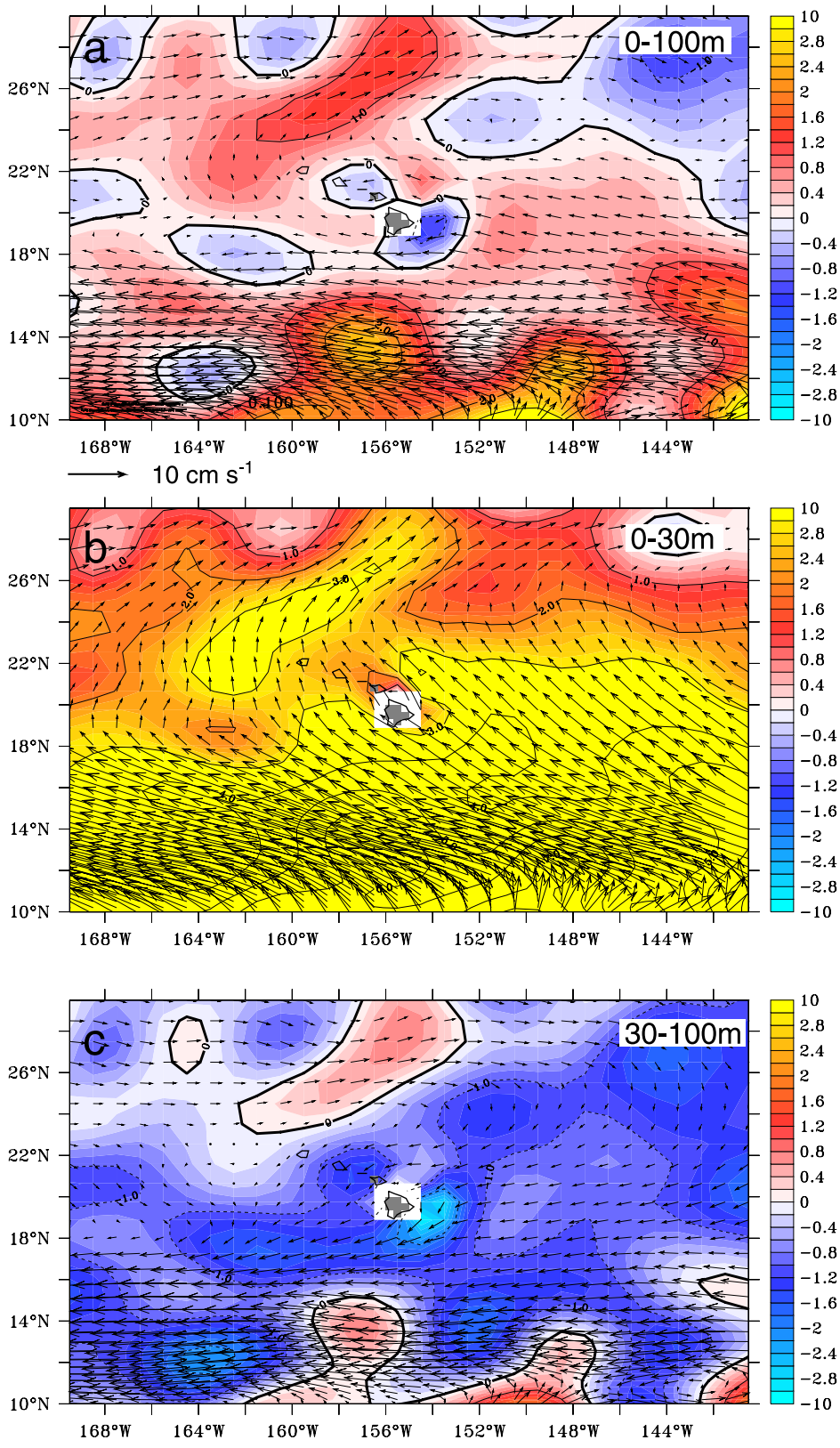

Figure 10. Maps of upper ocean circulation in the vicinity of Hawaii estimated by the ECCO reanalysis model [*Stammer et al.*, 2002]. (a) 0–100 m averages, (b) 0–30 m averages, and (c) 30–100 m averages. The vectors show the total velocity, while the contours show the magnitude of the meridional velocity component. Results are the annual averages for the 1997 to 2002 period as simulated by the adjoint version of the ECCO model. Units are cm s^{-1}.